SANDIA REPORT

SAND2017-6959
Unlimited Release
Printed July 2017

Determination of battery stability with advanced diagnostics

Joshua Lamb[1], Loraine Torres-Castro[1], Christopher J. Orendorff[1], Eric J. Dufek[2], Lee Walker[2], Chinh Ho[2]

Prepared by
Sandia National Laboratories
Albuquerque, New Mexico 87185 and Livermore, California 94550

Sandia National Laboratories is a multimission laboratory managed and operated by National Technology and Engineering Solutions of Sandia LLC, a wholly owned subsidiary of Honeywell International Inc. for the U.S. Department of Energy's National Nuclear Security Administration under contract DE-NA0003525.
Approved for public release; further dissemination unlimited.

Issued by Sandia National Laboratories, operated for the United States Department of Energy by National Technology and Engineering Solutions of Sandia.

NOTICE: This report was prepared as an account of work sponsored by an agency of the United States Government. Neither the United States Government, nor any agency thereof, nor any of their employees, nor any of their contractors, subcontractors, or their employees, make any warranty, express or implied, or assume any legal liability or responsibility for the accuracy, completeness, or usefulness of any information, apparatus, product, or process disclosed, or represent that its use would not infringe privately owned rights. Reference herein to any specific commercial product, process, or service by trade name, trademark, manufacturer, or otherwise, does not necessarily constitute or imply its endorsement, recommendation, or favoring by the United States Government, any agency thereof, or any of their contractors or subcontractors. The views and opinions expressed herein do not necessarily state or reflect those of the United States Government, any agency thereof, or any of their contractors.

Printed in the United States of America. This report has been reproduced directly from the best available copy.

Available to DOE and DOE contractors from
U.S. Department of Energy
Office of Scientific and Technical Information
P.O. Box 62
Oak Ridge, TN 37831

Telephone: (865) 576-8401
Facsimile: (865) 576-5728
E-Mail: reports@osti.gov
Online ordering: http://www.osti.gov/scitech

Available to the public from
U.S. Department of Commerce
National Technical Information Service
5301 Shawnee Rd
Alexandria, VA 22312

Telephone: (800) 553-6847
Facsimile: (703) 605-6900
E-Mail: orders@ntis.gov
Online order: http://www.ntis.gov/search

SAND2017-6959
Unlimited Release
Printed July 2017

Determination of battery stability with advanced diagnostics

Joshua Lamb, Leigh Anna Steele and Christopher J. Orendorff
Department Names
Sandia National Laboratories
P.O. Box 5800
Albuquerque, New Mexico 87185-MSXXXX

Eric J. Dufek, Lee Walker, and Chinh Ho
Energy Storage and Advanced Vehicles Department
Idaho National Laboratory
P.O. Box 1625
Idaho Falls, ID 83415-MS3750

Abstract

Lithium ion batteries for use in battery electric vehicles (BEVs) has seen considerable expansion over the last several years. It is expected that market share and the total number of BEVs will continue to increase over coming years and that there will be changes in the environmental and use conditions for BEV batteries. Specifically aging of the batteries and exposure to an increased number of crash conditions presents a distinct possibility that batteries may be in an unknown state posing danger to the operator, emergency response personnel and other support personnel. The present work expands on earlier efforts to explore the ability to rapidly monitor using impedance spectroscopy techniques and characterize the state of different battery systems during both typical operations and under abusive conditions. The work has found that it is possible to detect key changes in performance for strings of up to four cells in both series and parallel configurations for both typical and abusive response. As a method the sensitivity for detecting change is enhanced for series configurations. For parallel configurations distinct changes are more difficult to ascertain, but under abusive conditions and for key frequencies it is feasible to use current rapid impedance techniques to identify change. The work has also found it feasible to use rapid impedance as an evaluation method for underload conditions, especially for series strings of cells.

ACKNOWLEDGMENTS

This work was funded by the United States Department of Transportation, National Highway Traffic Safety Administration. We would like to thank our project sponsors Mr. Phillip Gorney and Mr. Stephen Summers.

This work was prepared as an account of work sponsored by an agency of the United States Government under INL Contract # DE-AC07-05ID14517.

Sandia National Laboratories is a multimission laboratory managed and operated by National Technology and Engineering Solutions of Sandia LLC, a wholly owned subsidiary of Honeywell International Inc. for the U.S. Department of Energy's National Nuclear Security Administration under contract DE-NA0003525.

We would like to thank Jon P. Christophersen, Christopher Hendricks and Scott W. Spangler as past contributors to this project.

We would like to thank other members of the Sandia Technical team including Leigh Anna M. Steele, June Stanley, Christopher Grosso and Jerry Quintana.

CONTENTS

FIGURES

NOMENCLATURE

[Sample list:]

BMS	Battery Management System
dB	decibel
DOE	Department of Energy
EIS	Electrochemical impedance spectroscopy
SNL	Sandia National Laboratories
SOC	State of charge
SOH	State of health
SOF	State of functionality
IMB	Impedance measurement box
INL	Idaho National Laboratory

1. INTRODUCTION

Traditional monitoring of electrochemical cells and batteries has been limited to observation of voltage and sometimes temperature of the cell or cells. While this monitoring can be very robust, there are limits to how predictive voltage and temperature behavior can be prior to a thermal runaway event. Ultimately, voltage and temperature changes are often lagging indicators of battery failure, and by the time a noticeable change is detected it is too late to arrest cell failure with intervention or maintenance. Further, instantaneous voltage and temperature monitoring are often inadequate to determine the state of a battery at rest, particularly if the battery has been previously subjected to an abusive condition. Proper handling of a battery after an abusive event generally requires assuming the battery is potentially unstable and may yet undergo a thermal runaway event. This usually requires full discharge and/or destruction of the battery after an abusive event whether a thermal runaway was observed or not. Knowledge of the level of stability of a damaged battery would allow for both safer and more efficient handling of the abused battery.

This work examines the application of Electrochemical Impedance Spectroscopy (EIS) as a tool for determining the state of stability of an electrochemical cell or battery. The cells for this study were subjected to thermal and electrical abuse coupled with EIS monitoring at differing levels of battery abuse. This aims to not only provide a deeper understanding of how abused cells and batteries fail, but also form the technical basis of a tool that could ultimately be used to interrogate cells of an unknown stability and even monitor active cells for early signs of damage or failure. These tests will look for markers within the EIS data that correspond to the onset of unstable conditions. These markers could then be potentially applied to interrogate batteries of an unknown stability as well as provide the basis for an active diagnostic method as part of a battery management system.

The primary drawback of traditional EIS is that it is typically not suited to measurements of dynamic systems due to the time involved to take a full measurement. This has historically limited the use of impedance measurements to either full spectra of stable systems, or dynamic measurements at a single high frequency, such as 1000 Hz. These have significant drawbacks, as limiting the measurement to stable systems would preclude any use as an on-board diagnostic tool, and single frequency measurements generally only yield limited information. Fast impedance techniques have been developed previously, but typically require expensive hardware and sophisticated data analysis to replicate the data obtained through traditional measurements. Idaho National Laboratories has developed a fast impedance tool that uses off the shelf parts. This tool is evaluated as part of this work, including both replicating the work performed with the traditional tool as well as collecting impedance data during dynamic conditions.

1.1. Stability of abused batteries

Abuse of electrochemical cells and batteries can have a wide range of effects depending on the type and severity of damage caused, as well as the properties of the battery itself. From a safety perspective, simple passive monitoring is often unable to identify the onset of failure until it is too late to intervene. Once a significant voltage change or self-heating of a cell is observed, a

catastrophic runaway of the cell is often inevitable [1-7]. The ultimate weakness of traditional monitoring techniques, typically based on voltage and temperature monitoring, is that they detect only the symptoms of a cell failure. Once a significant change has been registered, irreversible internal changes have likely already occurred within the cell. Compounding the issue is the fact that batteries have everything they need to release their stored energy inside the cell, meaning that once a catastrophic failure has initiated no amount of intervention can keep the reaction from proceeding to its conclusion. The prevention of catastrophic failure requires detection of internal faults well before they have developed to the point of no return. This makes techniques that can monitor the internal health of a cell essential to provide true protection from catastrophic failure. Further, many common forms of non-abusive field failure, such as internal short circuits, are the result of small defects that develop and exacerbate over time and are not readily detectible with conventional diagnostic tools at the time of a cell's initial construction. Monitoring changes to the impedance would aid in identifying ailing cells before a dangerous and costly failure.

Safety issues can be further compounded by the use of multi-cell modules. Monitoring of a pack of multiple cells with traditional techniques can be misleading as a pack that otherwise appears healthy may have a single problematic cell within the pack. Abusive conditions can also be unintentionally created, as voltage imbalance can create overcharge and overdischarge conditions while poor thermal design of a module can create thermally abusive conditions. A single cell undergoing catastrophic failure can cause cascading failures to other cells within the module.

These problems present a clear need to be able to detect and mitigate catastrophic cell failure under normal use and abuse conditions for transportation energy storage systems. Figures 1 through 3 show testing results for a series of lithium-ion cells under overcharge, mechanical penetration, and thermal abuse conditions. Under each abuse scenario, the failure events are preceded by a cascading sequence of decomposition reactions that are a challenge to monitor using passive temperature and voltage measurements. In general, voltage and/or temperature signatures indicative of failure are measured well after the point where these degradation reactions can be arrested and a failure event could be prevented.

Figure 1 shows an overcharge abuse test of a lithium-ion cell at 2C. In the region between 100 and 125% SOC the cell voltage increases by <400 mV and the temperature increases by 25°C. At 125% SOC, there is an inflection in both the voltage and temperature response of the cell, indicative of eminent, unstoppable failure. The cell becomes highly resistive and the cell voltage reaches the charging compliance voltage which is followed by a high order runaway and cell failure.

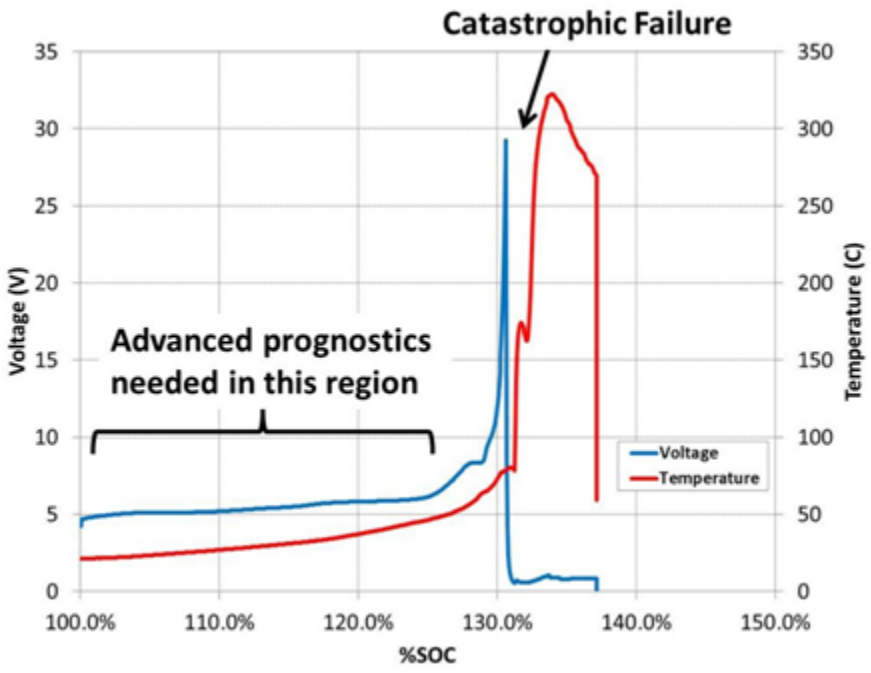

Figure 1 Cell voltage and skin temperature as a function of state-of-charge during a 2C overcharge test of a 12 Ah lithium-ion cell

In a slow speed, mechanical penetration experiment, there can be almost no passive warning signs prior to cell failure, shown in Figure 2. A cell in penetrated at 0.02 mm/s and shows no voltage drop or temperature rise during the first 4 mm of intrusion (up to 350 s). Once the cell package is ruptured, the cell short circuits and immediately goes into thermal runaway. Similarly, there is very little warning for a cell that develops an internal short circuit over time in the field because of a manufacturing defect or flaw which leads to a failure event [8]. During a thermal abuse scenario (Figure 3) there is a clear onset point of cell self-heating prior to a thermal runaway event. However, once appreciable self-heating is initiated it is practically too late to avoid a runaway reaction. In all of these abuse scenarios with conventional lithium-ion cell chemistries, rapid response, embedded sensors to measure internal cell degradation along with control strategies to remove the abuse and mitigate failure are essential. Early detection and prevention are critical for arresting these cascading degradation reactions that lead to an unstoppable runaway failure event.

Current state-of-the-art in battery monitoring for both industrial and on road motive power applications falls far short of the capability to detect impending battery failure. Rather, the state-of-the-art simply provides for operating the battery within a set of prescribed conditions to maintain optimal operation. Battery failures are detected only if the occur over a prolonged period and impact overall battery performance. Rapid failures are neither detected nor mitigated in the current state-of-the-art.

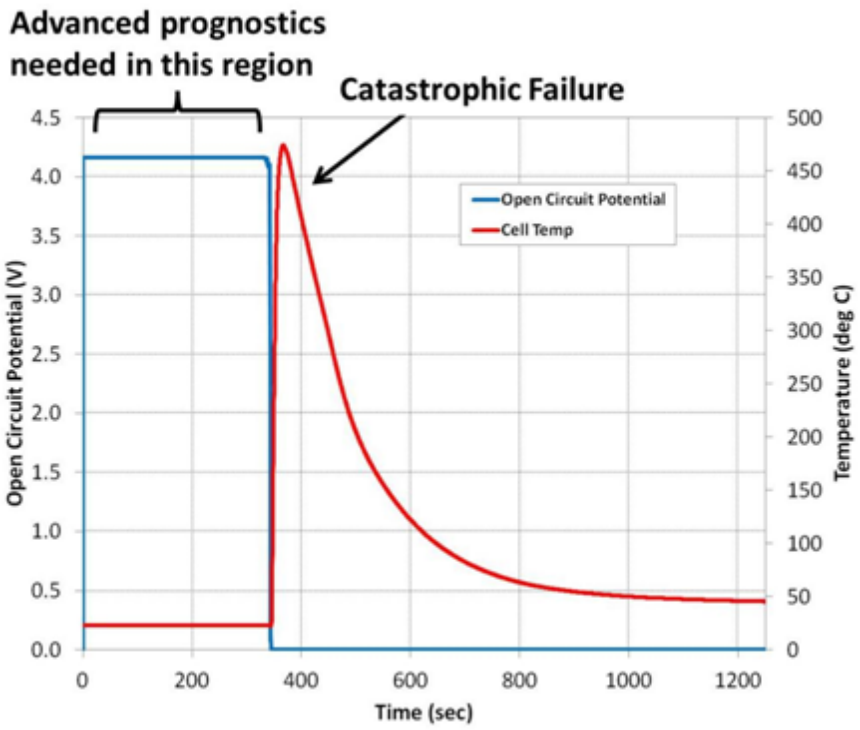

Figure 2 Cell voltage and skin temperature as a function of time during a blunt nail penetration test of a 2 Ah 18650 cell

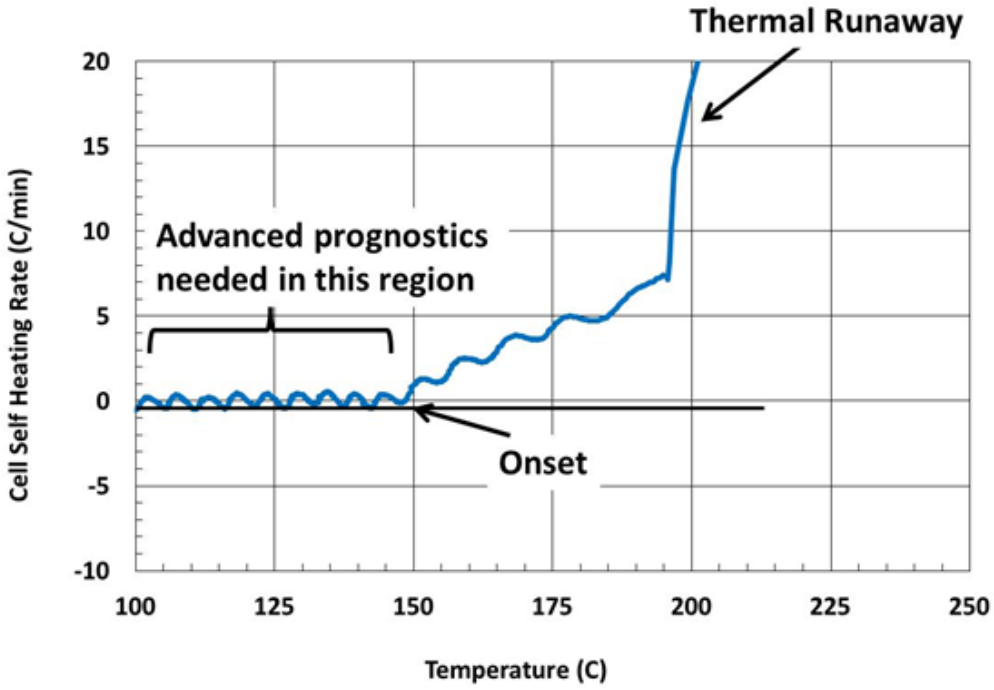

Figure 3 Cell self-heating rate (°C/min) as a function of temperature of a 2 Ah 18650 cell during a thermal ramp test at ramp rate of 5 °C/min

1.2. Electrochemical impedance spectroscopy

Electrochemical Impedance Spectroscopy (EIS) measurements have been emphasized as a valuable tool for battery modeling and life estimation [9-13]. AC impedance data have been shown to reveal changes in the bulk behavior of the electrochemical processes as well, which can give an indication of the changes in the battery electrode surface and diffusion layer [14]. With half-cells (i.e., using a reference electrode to isolate the individual effects of the anode and cathode during measurements [15], offline impedance measurements could also be a valuable diagnostic tool in assessing the degradation of the individual electrodes [16]. However, it has not been typically considered useful for online monitoring systems since the equipment is usually very expensive and the measurement duration is relatively lengthy. Standard AC impedance measurements usually consist of sequentially sweeping through a given frequency range by injecting sinusoidal excitation signals into the battery (or other energy storage device) and capturing the response. Depending on system settings and the frequency range, the impedance measurement sweep could last somewhere between 10 minutes to an hour, which is not well suited for onboard applications. Traditional impedance techniques may still be suited, however, to the evaluation of potentially abused batteries in an unknown state.

EIS is increasingly being used as well for estimation of the state of health (a measurement of performance degradation) and state of charge of batteries. Fleischer et al. [17, 18] have described algorithms for modelling the level of functionality based on parameters measured by the BMS. They suggested the use of EIS to monitor the charge transfer resistance, but conceded it was likely not feasible due to the hardware necessary to collect impedance data. Impedance measurements have also been used to monitor changes to internal temperature of cells. Srinivasan et al. [19] as well as Schmidt et al. [20] have correlated impedance measurements to the internal temperature of an electrochemical cell and used empirical correlations to allow single frequency impedance measurements to serve as a means to monitor individual cell temperature.

Recent work has also used EIS to examine the changes in cells in light to moderate levels of abuse. Love et al. have examined the impact of overcharge on the single frequency impedance of single cells [21] as well as 4 cell series strings [22].This was able to find a measurable shift in the 500 Hz impedance data as a cell was overcharged up to 135% total SOC. Single frequency impedance such as this has the advantage of being easily integrated into a system as it does not necessarily require costly hardware or computing analysis, and also at higher frequencies can be measured very quickly to provide a real time measurement.

Single frequency measurements are capable at measuring shifts in the internal resistance, such as those caused by sold electrolyte interphase (SEI) breakdown or damage to the separator, but those specific frequencies would need to be carefully selected as the whole spectra can shift with aging. Changes in other quantities, such as the charge transfer resistance and the conductivity of the battery electrolyte may show shifts in the complex impedance spectrum but little change in a single frequency analysis. This is particularly true if the single frequency analysis is at a relatively high frequency, as many phenomena only become apparent at lower frequencies.
A typical Nyquist curve measured from a commercially available lithium-ion cell is shown in Figure 6. The high frequency tail on the left side of the spectrum at frequencies greater than

251.2 Hz typically captures equipment artifacts [22] and is not shown in this figure. The point at which the high-frequency tail crosses the real axis is the ohmic resistance (R_O) within the battery, which includes the effects from the electrolyte, electrodes, tabs, etc. The semicircle in the mid-frequency region identifies the effective charge transfer resistance (R_{CT}), which is primarily influenced by the kinetic reactions at the electrodes due to an imposed constant voltage or current signal. The low-frequency tail on the right is known as the Warburg impedance that is caused by the diffusion of ions [15, 23]. The semicircle trough, identified at 1.26 Hz, is the measured transition point between the mid-frequency charge transfer resistance and the low-frequency Warburg tail. These data show changes in the bulk behavior of the electrochemical processes and can provide valuable insight into battery degradation mechanisms during aging.

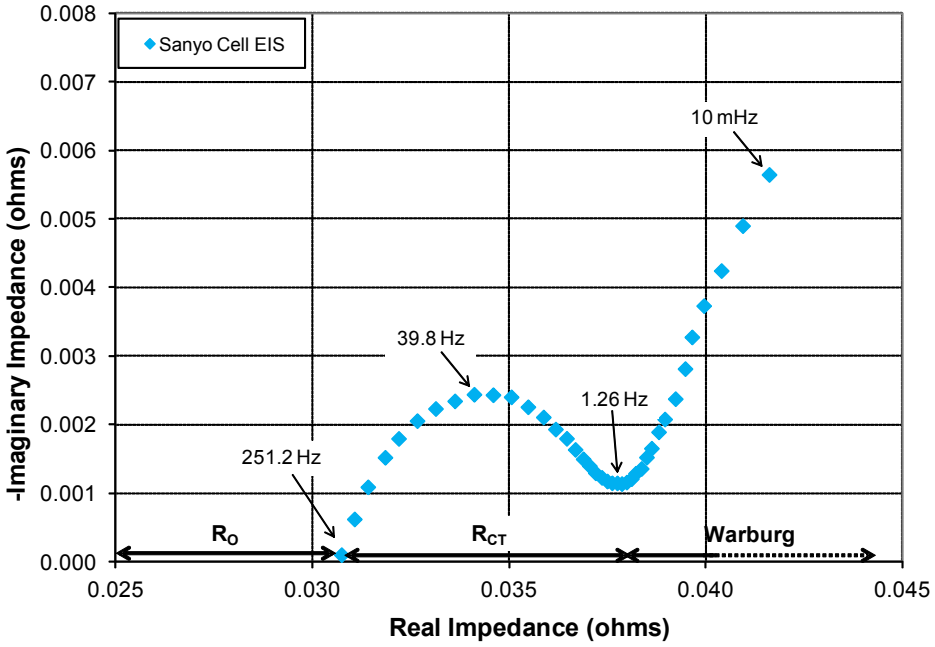

Figure 4 Impedance spectrum Nyquist curve for a single Sanyo SA Cell [22]

1.3. Fast impedance measurement tools

INL, in collaboration with Montana Tech of the University of Montana, has developed aprototype sensor to improve the overall accuracy and reliability of SOH assessment techniques for electrochemical energy storage devices. The principle of operation for this Impedance Measurement Box (IMB) is to capture impedance spectra rapidly over a broad frequency range using simple hardware and control software that processes unique algorithms to determine the spectra based on a sum-of-sines (SOS) excitation signal. Various rapid impedance spectrum measurement techniques have been developed to yield high resolution data comparable with standard, COTS equipment (i.e., multiple data points within the impedance spectra). Harmonic Compensated Synchronous Detection (HCSD) is an example of rapid, lower resolution impedance measurement technique [22, 24, 25]. The sum-of-sines excitation signal consists of frequencies that are separated by octave harmonics so as to eliminate the effects of crosstalk interference. With no crosstalk error, the duration of the excitation signal needs to be only one period of the lowest frequency. Thus, given a frequency range of 0.1 to 1638.4 Hz with 15 frequencies included within the sum-of-sines excitation signal (i.e., 0.1 Hz, 0.2 Hz, 0.4 Hz,

0.8 Hz, etc.), the measurement duration would only be ten seconds long. The overall battery response to the excitation signal is captured and then synchronously detected at each frequency of interest to determine the impedance spectrum. The analysis methodology is relatively computationally simple using synchronous detection without the need to compensate for crosstalk error and could be implemented as an embedded software analysis tool.
Because battery failure under abusive conditions occurs rapidly (several seconds to 10s of seconds) and can be destructive to the cell, analysis is typically limited to what can be passively measured in real time or what can be gleaned from the aftermath of a test. Measurement of impedance changes in failed cells is typically a before-and-after scenario, or not realistically possible due to the physical state of the cell after testing. The IMB sensor development may, however, also be used for rapid online assessment of battery failure mechanisms, allowing for in-situ characterization of impedance changes of a cell during failure and potentially lead to a greater understanding of the mechanisms of battery failure so as to prevent catastrophic events.

The successful development of a rapid impedance spectrum sensor that can help to improve the overall safety and reliability of batteries in addition to creating an opportunity for improved power management, monitoring, and control could significantly leapfrog existing approaches and have a positive impact on both technology and business aspects. For example, improved safety mitigation and control can help to reduce the potential for fires caused by thermal runaway that can result from conditions ranging from cell defects to automotive crashes.

[Blank page following section.]

2. EXPERIMENTAL METHODS

Cells in string configurations were evaluated in both series and parallel configurations. The base cell type for both series and parallel configurations was a 1.2 Ah Sanyo SA which is an 18650 format. The operational window for single Sanyo SA cells is between 2.5 and 4.2 V. These cells have been previously well characterized for both impedance purposes and for aging and life analysis at INL and are a good test case for multi-cell string configurations. Impedance evaluation was performed using a 48V version of the INL developed fast impedance tool (IMB).

2.1 Cell Aging

To understand the impact that different aged cells had on impedance response a set of cells was aged at 55°C using a cycling profile between the minimum and maximum voltage at a C/1 rate. Cells were aged to roughly 29% fade from their initial, experimentally determined capacity of 1.25 Ah. Following aging cells were discharged to their minimum voltage and held at that voltage until a C/100 current (0.012 A) was obtained to ease string configuration.

2.2 Four cell string testing

Prior to configuring strings all cells were discharged to their minimum voltage and held at that voltage until a C/100 current (0.012 A) was obtained. Cells were not placed in a string configuration until just prior to testing. An example of a configured string in its test fixture is shown in Figure 5. For the electrical evaluation of impedance and cell performance all measurements were performed in a controlled environmental chamber with the temperature at 30°C.

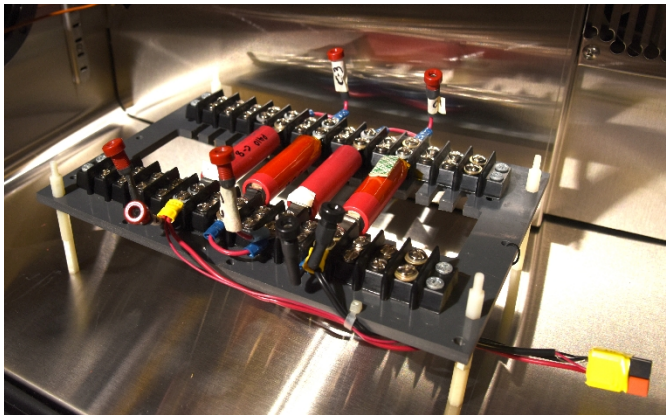

Figure 5 A four cell string configured for impedance analysis under both no-load and various underload scenarios.

To ensure reproducibility of measurement location during underload conditions a plot of the OCV versus the SOC of the cell was constructed. From this plot the voltage which equated to 25, 50 and 75% SOC were identified and used for both fresh and aged string configurations. For the 4S1P string the voltages were multiplied by four as shown in Figure 6.

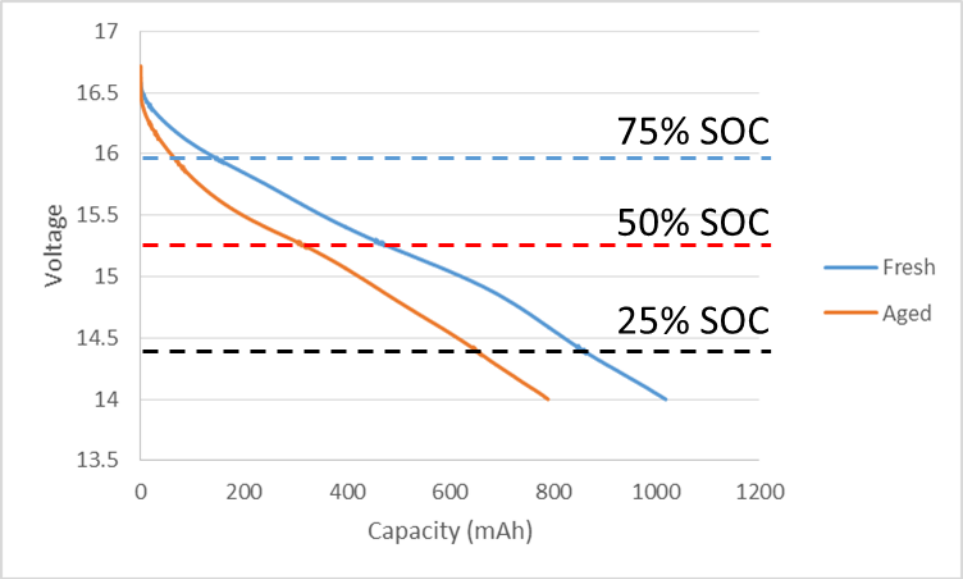

Figure 6 Voltage profile for the 4S1P string with four fresh cells and for 2 fresh and 2 aged cells

2.2.1 Series Configurations (4S1P)

The series strings were constructed by connecting four 1.2 Ah Sanyo SA cells in series. The 4S1P string had a maximum voltage of 16.8 V and a minimum voltage of 10.0 V. A series of impedance evaluations were performed on the cells to understand how the impedance signature varies as a function of state-of-charge and load condition. The different test conditions are shown in Table 1. The test matrix also incorporated two different string conditions one in which the string was constructed using all fresh cells and one where the string consisted of two fresh and two cells aged as described above. Impedance testing was performed using the IMB as described below.

Table 1 Test conditions for IMB characterization

Test Condition	***Impedance Data Acquisition Points***	***Current, A (Parallel String values)***
1) No Load	0, 25, 50, 75, and 100% SOC	0 (0)
2) Constant Current (C/3)	0, 25, 50, 75, and 100% SOC	0.4 (1.6)
3) High Current Charge Evaluation (1.8 C)	At 0, 10 and 20 min during charge	2.15 (8.6)
4) High Current Discharge (1.8C)	75%, 50% and 25% SOC	2.15 (8.6)

2.2.2 Parallel Configurations (1S4P)

Parallel strings were also constructed using four of the Sanyo SA cells. This produced a fully parallel string with a minimum voltage of 2.5 V and a maximum voltage of 4.2 V. The rated charge capacity of the parallel string was 4.8 Ah. As with the series string two different aging conditions were evaluated. One in which all four cells were fresh and one with two fresh and two aged cells. The conditions evaluated using the parallel string are also shown in Table 1 with the current and power values for the parallel conditions in parenthesis.

2.3 Testing with the INL fast impedance measurement tool (IMB)

Rapid acquisition of impedance data was performed using a rapid impedance measurement tool first developed at INL. The impedance measurement box (IMB) measurements were for frequencies ranging from 0.1-1638 Hz. The IMB used for data was of the third generation of the tool and had a maximum operating window of 48V.

For no load measurements the string was charged to a set voltage for each SOC level as determined from a single cell open circuit voltage (*OCV*) vs SOC diagram. The cell was then put into a rest state and the impedance data was acquired followed by further charging or discharging of the cell. For all charge measurements the SOC was collected in a consecutively increasing manner and for the discharge measurements the SOC was consecutively decreasing.

For underload conditions the measurements were started when the appropriate voltage from the SOC diagram was reached. During the measurement the load on the string was maintained. As with the no load measurements the data was acquired with an increasing SOC for charging events and a decreasing SOC for discharge measurements.

3. RESULTS

3.1 Commissioning of 50V impedance measurement box at Sandia National Laboratories

A 50V version of the impedance measurement tool (50VIMB) was commissioned and delivered to Sandia as part of this project. The 50VIMB was tested against a Solartron Modulab potentiostat to verify the comparability of measurements collected to traditional impedance collection tools. The data shown in Figure 7 was collected on both measurement devices on a Sanyo 1.2 AH 18650 cell. The data collected between both tools were in good agreement with each other, particularly showing near identical internal cell resistance and charge transfer resistance values.

This test has been periodically repeated throughout the project to ensure the data collected from the 50VIMB remains in good agreement with traditional measurements. No significant drift of the collected impedance data has been observed to date.

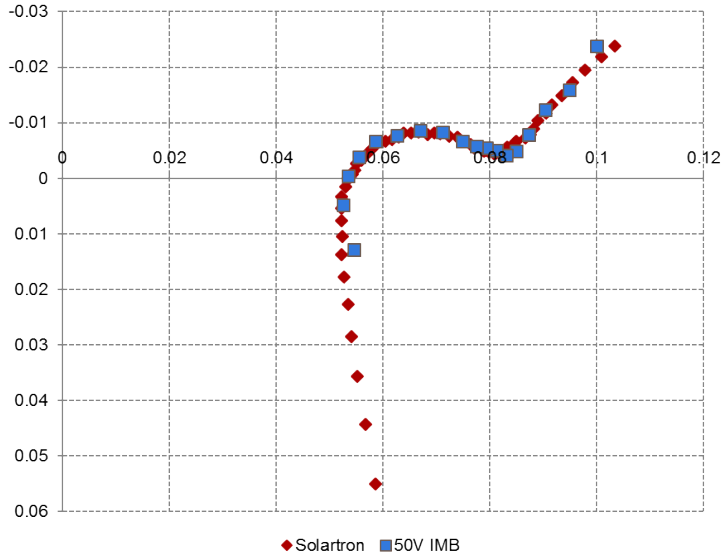

Figure 7 Validation testing of 50V IMB after commissioning at SNL. Comparison run on Sanyo 18650 cell to confirm equivalent data between traditional impedance testing and 50V IMB testing hardware.

3.2 Electrical Evaluation of String Configurations

As shown in Table NN the evaluation of scenarios for both parallel and series strings were evaluated using the IMB. These scenarios were designed to provide a first analysis of the suitability of using the IMB for evaluation of battery state during possible anticipated scenarios such as during a fast charging event, during rest and as a tool for diagnostics during the discharge of a battery using two different constant currents. A key reason for the analysis during a discharge event is as a possible route for first responders and other support personnel to evaluate a battery in an unknown condition such as after a wreck or after/during storage in a salvage yard.

It is well known that strings of cells configured in parallel and series fashion exhibit significantly different impedance response as shown in Figure 8. The dramatic difference in conditions requires that the analysis of the response associated with series and parallel configuration be performed separately.

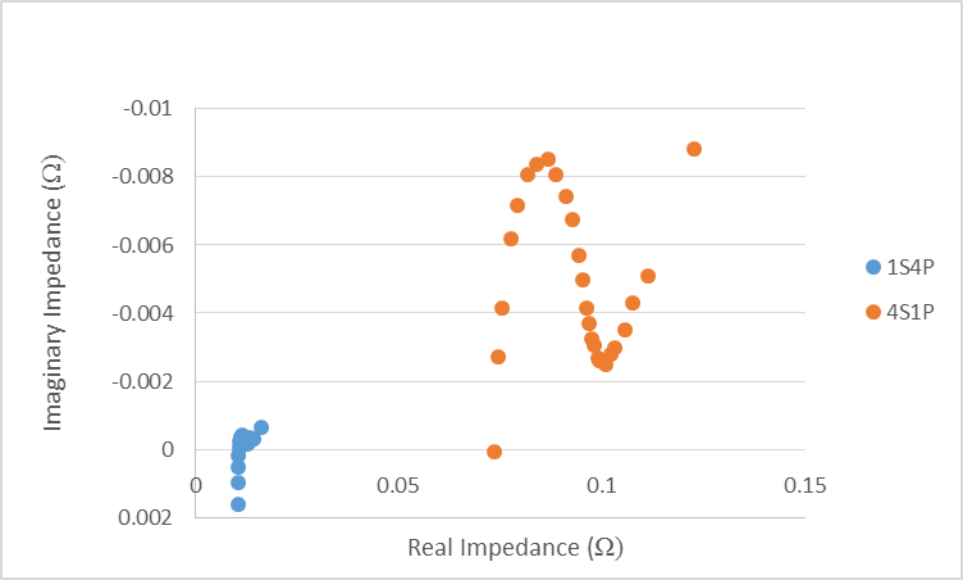

Figure 8 Comparison of the Nyquist plots for a 1S4P and a 4S1P string of 18650s at 25% SOC.

3.1.1 Parallel Configurations

One of the most popular means to plot impedance data from EIS and similar methods is through the use of a Nyquist plot. While this is advantageous for single or a few sets of data it becomes unwieldly for the analysis and visualization of larger data sets. Another means to present the data obtained is by plotting the complex magnitude of the impedance for each of the respective frequencies as shown in Equations 1.

$$|z| = \sqrt{ReZ^2 + ImZ^2} \qquad \text{Equation 1}$$

Recall from Figure 8 that there are distinct regions which are associated with different processes occurring in a battery. For the 1S4P cell string the frequencies which correspond to R_O vary between 204 and 307 Hz for the present cells while the frequency corresponding to the transition from the charge transfer to the Warburg region is 3.2 Hz. For analysis purposes all frequencies above 307 Hz and below 3.2 Hz were removed for two reasons. First the high frequencies are more prone to influence from issues such as cabling and equipment artifacts [24]. For the low frequency range, one of the concepts was to use the IMB technology while the system is underload. When the system is underload, the diffusion of ions is impact by both the SOC as well as the load being applied, thus the low frequency items were also excluded.

Within the range of frequencies identified for analysis (3.2-307) it is necessary to understand the variability associated with equipment that occurs between measurements. The ability to quantifiably know the variance in measurements at a certain state is what enables detection limits

for instrumentation to be assessed and what is necessary when a signal such as impedance is used for diagnosing the health or safety of a battery. For this reason data was acquired for the parallel string. For many diagnostic purposes the limit of detection (LOD) equates to values that are at least three times the standard deviation away from the average of a set of measurements. When applied to the present data the maximum value for the LOD for the frequencies of interest is on the order of 2.2×10^{-4} Ω for complex impedance measurements. Thus, when the IMB signal is being used to identify if there is a detectable variance from the base signal the difference in z between the baseline condition (no-load, no aged cells) and the signal of interest (either underload or with aged cells) needs to be at least 2.2×10^{-4} Ω different than the base signal.

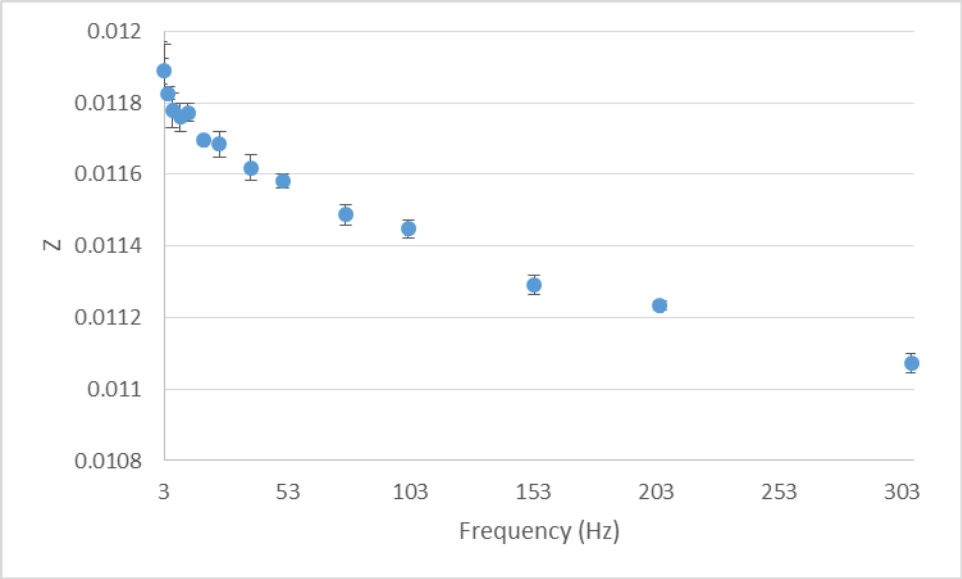

Figure 9 Average z values with standard deviation bars included for five independent measurements for the 1S4P string under a no-load condition prior to the start of a charge (0% SOC).

With an understanding of the variance that needs to be seen between signals in mind the baseline condition data was collected for a string of cells that had no aged cells and was not underload. Figure 10 contains the data collected for the 1S4P string under the no load condition. For both the charging and the discharging of the parallel string there is sufficient change across the range of SOCs in the complex impedance signal to allow further analysis of the data. Figures 11 and 12 present two different experiments which were conducted to discern the ability to monitor changes to the condition of the parallel string.

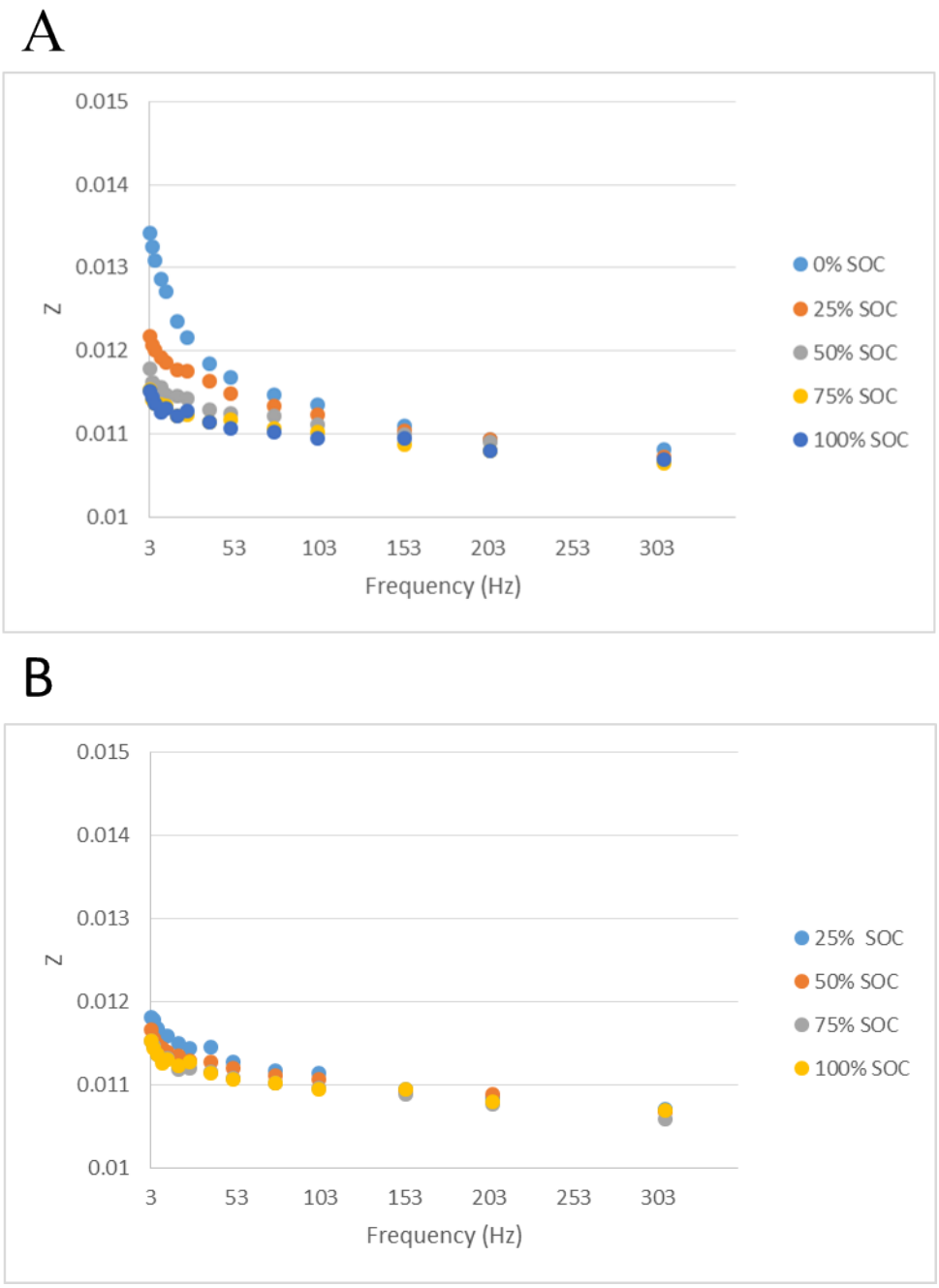

Figure 10 The z data for a 1S4P string under no-load at various SOCs.

In Figure 11 the difference in z (Δz) for different SOCs is shown for the condition where the cells within the string were either all fresh or where two cells within the string were aged. For each of the different states of charge there is a distinct difference between the two conditions and for all frequencies of interest and for all SOCs the difference between the baseline condition and the aged condition fall above the LOD. However, there variance for each instance falls well

below the levels typically seen for a limit of quantitation (LOQ) which is typically defined as 10 times the standard deviation of baseline measurements.

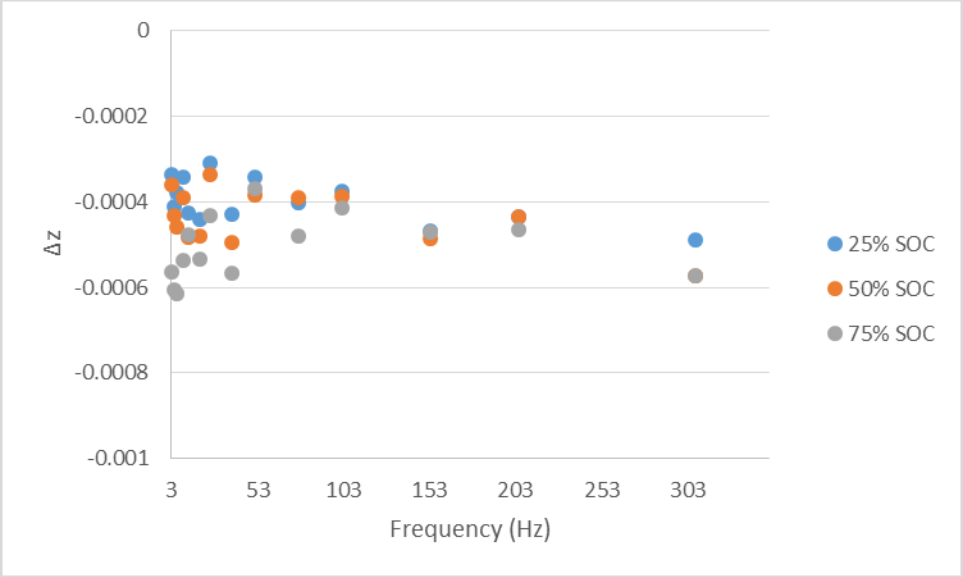

Figure 11 Complex impedance difference between a 1S4P string that contains four fresh and two fresh and two aged cells.

As opposed to the aged and fresh data in Figure 11, the difference between data collected under load at a 1.8C rate and under a no-load condition for four fresh cells in a 1S4P configuration only partially exceed the LOD (Figure 12). Indeed, at both 25% and 50% SOCs there are only a few points which exceed the 2.2 x 10^{-4} Ω LOD. Even at 75% SOC the values all fall well below the LOQ.

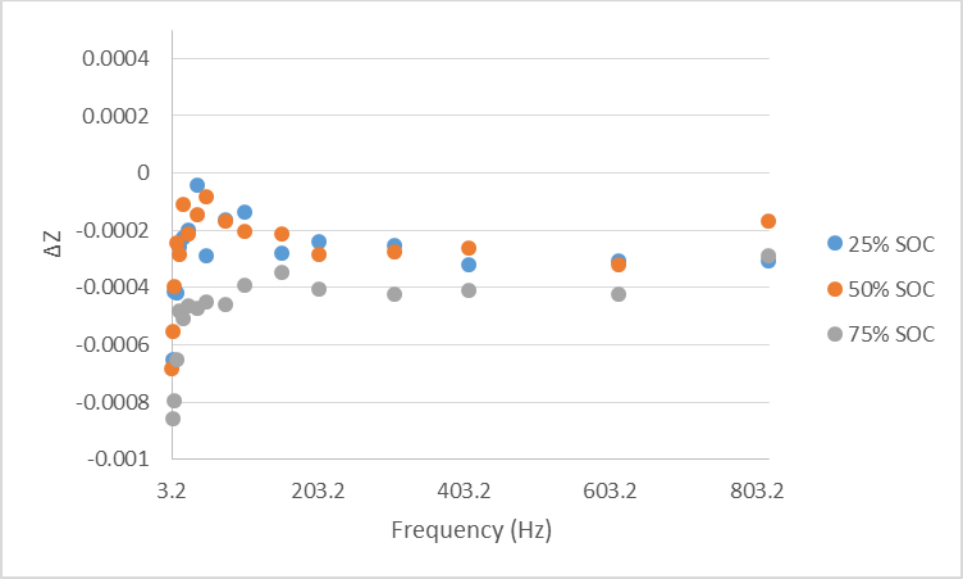

Figure 12 Complex impedance difference between a 1S4P string in a no-load condition and during discharge at a 1.8C rate.

Given the data in Figures 11 and 12 it is evident that for parallel configurations the ability to quantify distinct changes in strings is not feasible (at least to the extent of variance seen for these conditions). The impact of the inability to quantify differences between conditions for parallel strings is such that clearly distinguishing may not be possible for the present set of conditions. However, routes to improve the measurement-to-measurement variability are feasible. These include longer measurement times which exceed the present 10 second data acquisition and greater signal averaging. That said, the fact that several discrete frequencies exceed the LOD indicates that while quantification is not feasible, identification and detection of a change in condition is possible even for 1S4P cell configurations.

3.1.2 Series Configurations

The nature of series configurations is such that changes in impedance are significantly easier to detect. The data indicates that for the higher frequencies greater than 350 Hz there is not significant difference as a function of SOC though there is a difference for the aged versus fresh condition. At the lower frequencies, which occur near R_{CT} there is sufficient difference to clearly discern both aging condition and SOC.

Not only are there distinct population for fresh and aged cells under no-load conditions the variation also exists for the series strings during high rate discharge. For the high rate discharge (1.8C) the difference for each SOC is less well defined across the different complex impedance values for the aged cells, though for fresh cells there is slight difference between the three SOCs shown here. Recall that complex impedance includes both real and imaginary components. This

provides the opportunity to look at three different set of signals for characterizing the state of a string of cells.

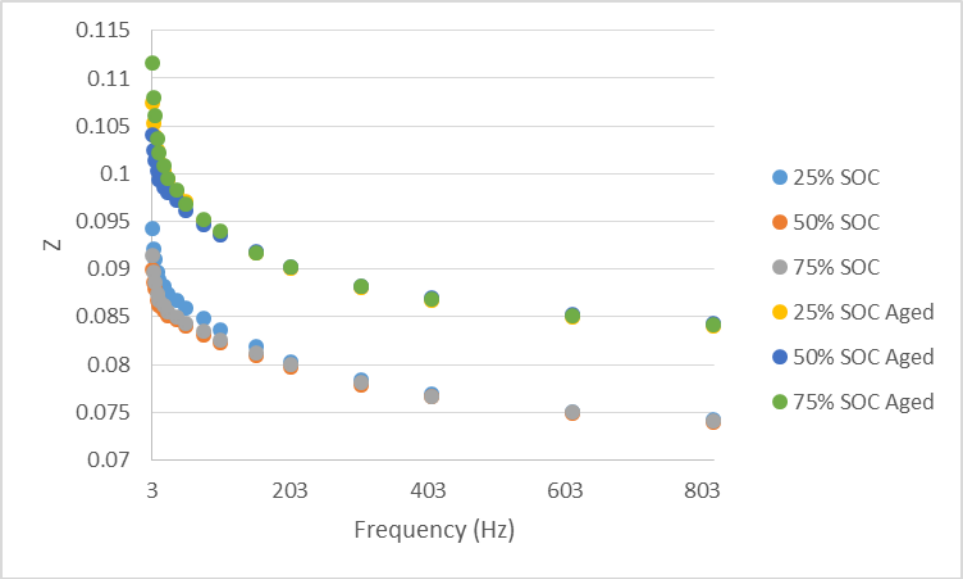

Figure 13 Complex impedance during discharge (1.8C) at three different SOCs for a string (4S1P) with four fresh cells and with two aged and two fresh cells.

For both no load and underload measurements there are two distinct populations which correspond to the aged and fresh cells. However, for the string with two aged cells there is less differentiation between the states of charge, when considering the complex impedance, than there is for the 4S1P string with four fresh cells. When just the real component of the impedance are considered and the difference between SOCs is clearly visible for both fresh and aged cells (Figure 14). From the combination of the data in Figure 13 and 14 it becomes possible to distinguish both age and SOC for the cells not only from a detection standpoint but both are sufficiently above the LOQ.

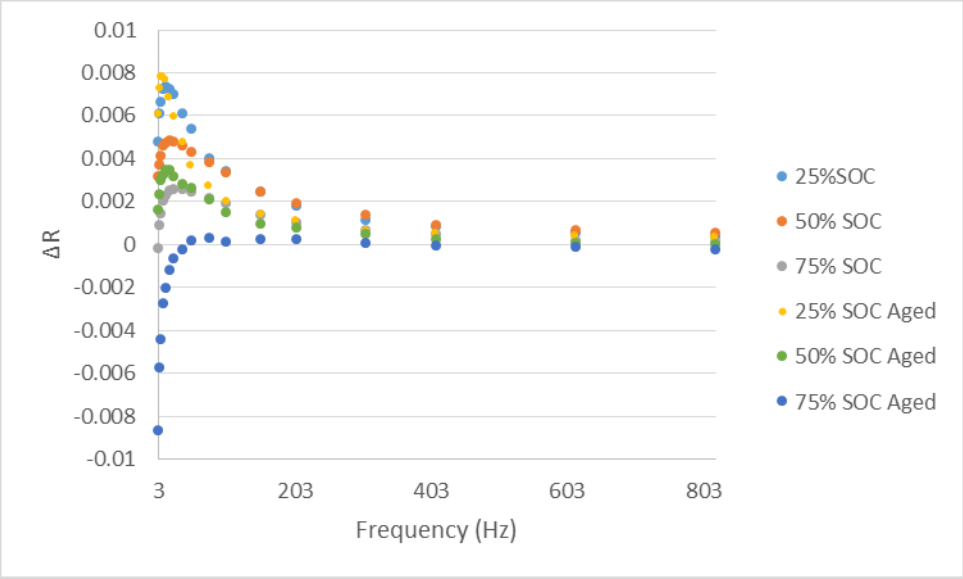

Figure 14 The difference in real impedance (R) for a no-load and a 1.8C measurement for a 4S1P string consisting of either 4 fresh or 2 fresh and 2 aged cells.

For series strings it is distinctly possible to both detect and quantify differences in signal when using both the real and the complex impedance. This is varies from parallel strings where only detection of variance is possible for the present experimental set up. Going forward it is necessary to better understand how series configurations of different cell types and how complex strings which are configured in both series and parallel impact detection.

3.1.3 Abusive battery tests in series packs

The more prominent results in pack tests with series measurements were observed when coupled with abuse testing procedures as well. The use of the high voltage IMB hardware allowed for the real time monitoring of series packs during the application of a thermal ramp abusive test to a single cell within the pack. The results of this test are shown in Figures 15. This data shows a strong trend in the pack as a single cell overcharge is applied. Initial heating of the cell from 25-75 °C shows minor changes to the internal resistance of the cell, with larger changes observed in the internal resistance as the abused cell temperature increases up to 110 °C, however at these temperatures the general behavior of the battery is similar to the lower temperature behavior.

At 120 °C and above, as shown in Figure 16 there is a significant shift in the behavior of the data. At this point the pack becomes significantly more resistive, with a jump from ~110 mOhm to ~140 mOhm. Further, the pack loses much of its capacitance, showing a trend similar to what would be expected of an imperfect resistor. This seems to indicate that at these temperatures the cell has lost the bulk of its energy storage capability and may be damaged beyond any functionality.

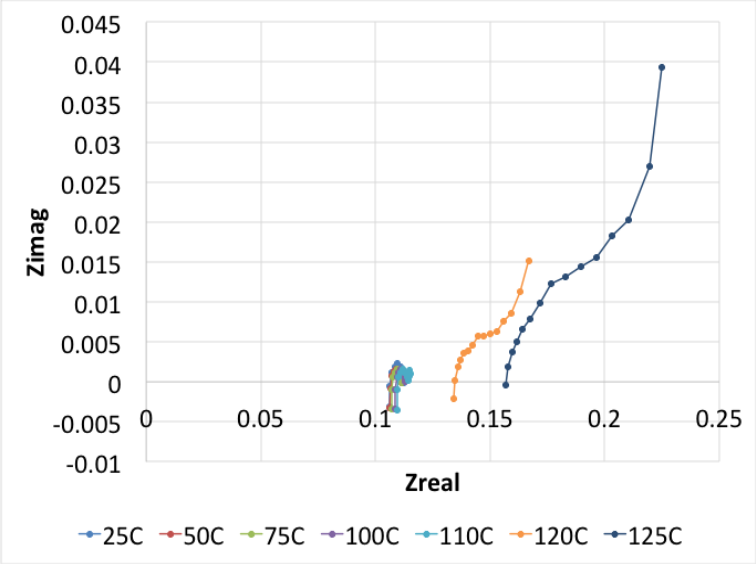

Figure 15

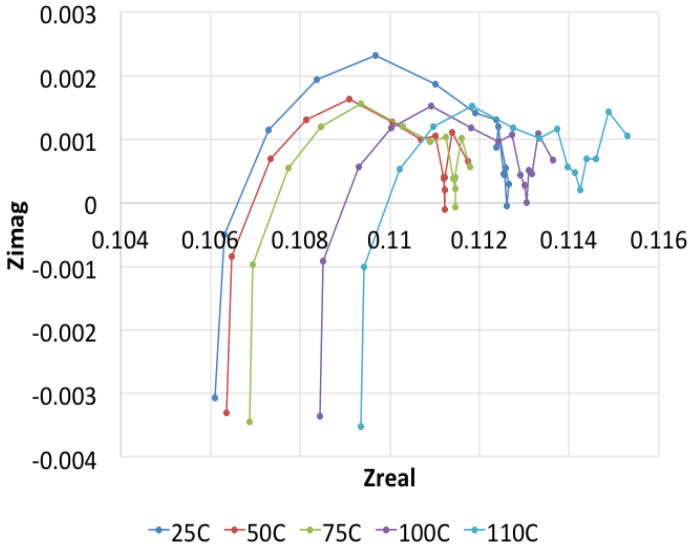

Figure 16

3.1.4 Testing of real time impedance measurements coupled with an operating BMS system

Applying these diagnostic techniques in a real world situation requires testing alongside Battery Management System (BMS) hardware. Impedance testing requires an injection of a small amount of current into the system in order to generate data. The presence of the extra circuitry that accounts for an operating BMS may alter the results of the impedance tests. At the same time, the BMS is required for the safe functioning of the system. It is imperative that the use of any monitoring technique not interfere with the regular operation of the BMS.

Packs were built with a commercially available BMS (http://www.orionbms.com) wired to the pack. Initial testing compared impedance data collected on a single cell wired in parallel with the

BMS system. The results of this initial impedance scan are presented in Figure 17. This shows a small drop in the measured internal resistance with other aspects of the data remaining largely the same after adding the BMS. This is likely due to the small amount of current that is drawn by the BMS as part of its normal operation.

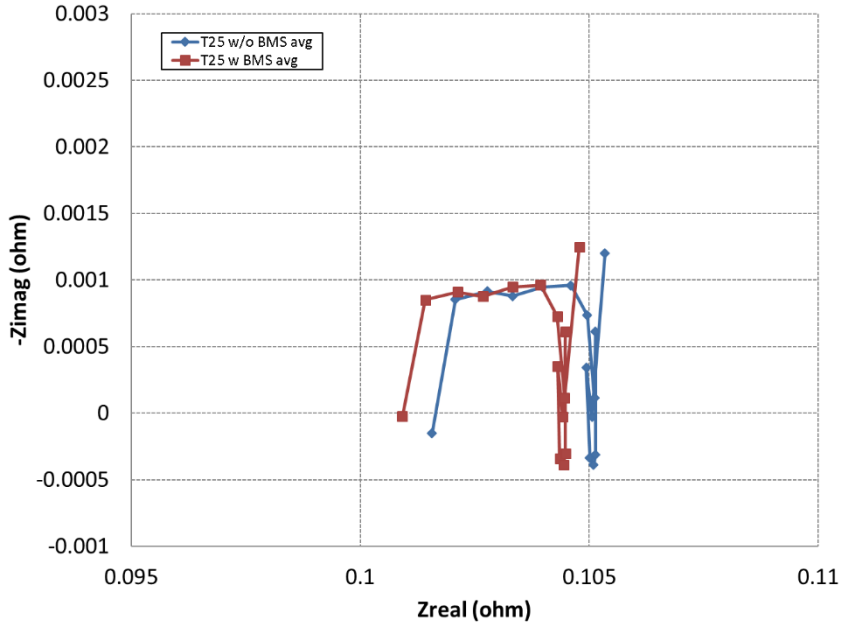

Figure 17 Comparison of ambient temperature impedance scan with and without BMS in use

After this initial testing a single cell was tested with the BMS is use. These results are shown in Figures 18-20. The abuse and voltage data in Figure 18 show a measurable voltage drop in the cell beginning above 100 °C and an onset of runaway at ~ 200 °C. The BMS hardware also monitored the cell voltage through the duration of the test with this data shown in Figure 19. This shows some interference in the BMS monitored voltage from the activity of the impedance measurement, particularly as the cell reached higher temperatures.

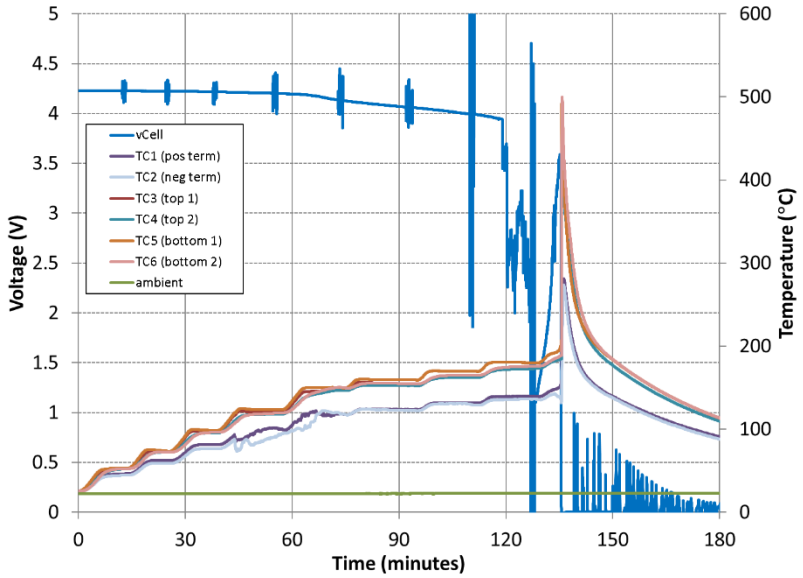

Figure 18 Abuse test of a single cell coupled with impedance monitoring and BMS hardware moitoring

At higher temperatures, the cell became more sensitive to the signal injection generated for impedance measurement, which created measurable voltage signals in the BMS measurement. This could likely be compensated for within an on board BMS, for example by disabling the voltage measurement whenever an impedance measurement was taken. It is still something that would need to be accounted for if integrating an active signal measurement technique like impedance measurements into an on board system.

Impedance measurements recorded up to 125 °C are shown in Figure 20. This shows some trends similar to those seen in previous data above, however the presence of the BMS does introduce some noise to the measurement. Minor changes are observed up to ~75 °C tied to increases in cell temperature. At higher temperatures, more significant changes are observed in the data with significant changes observed in both the charge transfer resistance and internal cell resistance.

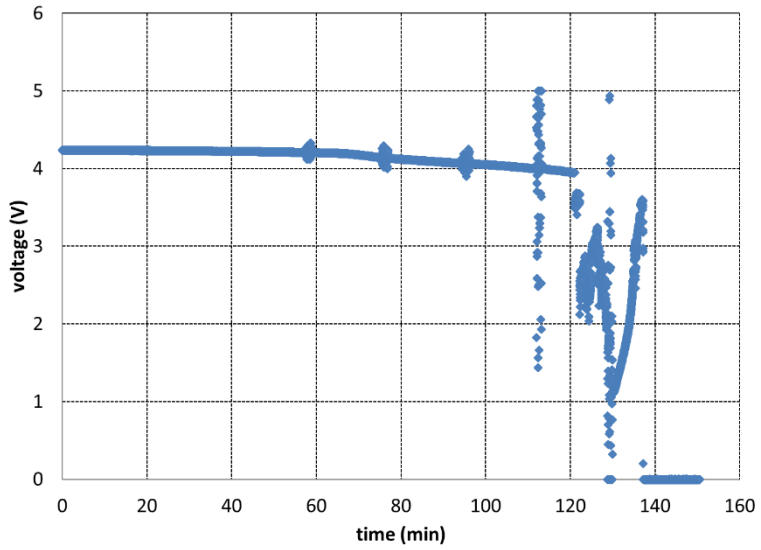

Figure 19 BMS monitoring of cell tested in Figures 18

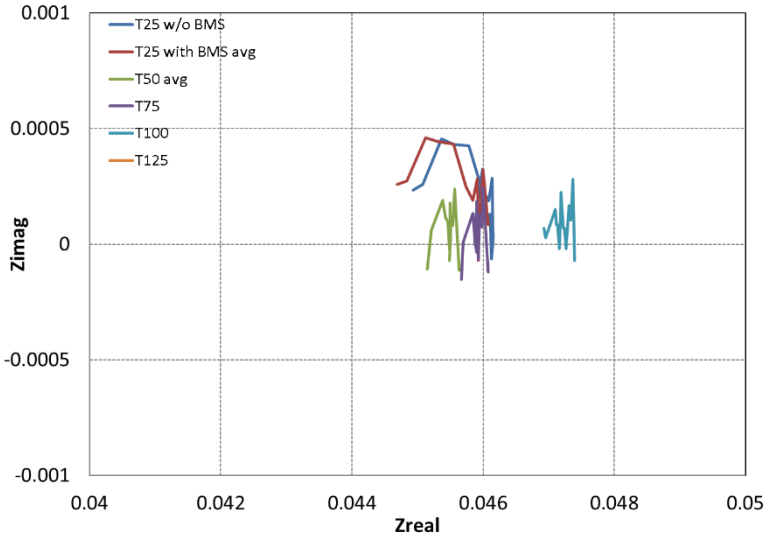

Figure 20 Impedance data collected during abuse testing of a single cell in parallel with BMS system.

This test was performed as well with the BMS monitoring a three cell series (3S1P) string of cells. In this case the BMS was configured to monitor cells all cells within a three cell string while a thermal ramp abuse condition was applied to cell 2. The results of the abusive test are shown in Figure 21. The temperatures of the thermally abused cell are shown, along with pack voltage and all individual cell voltages. The BMS data was logged as well and is shown in Figure 22. This data shows similar behavior to the single cell data. Perturbations in the monitored voltage are observed in both Cell 2 and the overall pack voltage, due to the signal injection performed during impedance measurement.

Impedance monitoring collected during this testing is shown in Figures 23 and 24. This data shows similar results to that observed in other three cell series packs. Specifically, smaller changes are observed as the cell 2 is heated up to 100 °C, while at 125 °C and above significant changes are observed in both the cell resistance and the overall behavior of the impedance spectrum. Similar to previous data, this suggests that significant permanent and immediate changes are made to the cell when it rises above 100 °C. Below that point while the cell may be suffering damage that leads to long term instability or unreliability, the immediate concern is not as great. Further, this data shows that the presence of the BMS has little impact on the impedance measurements. There is, however, some noticeable signal that appears on the data logged by the BMS itself. This is something that would have to be considered in the software design of the BMS if used with an operating battery.

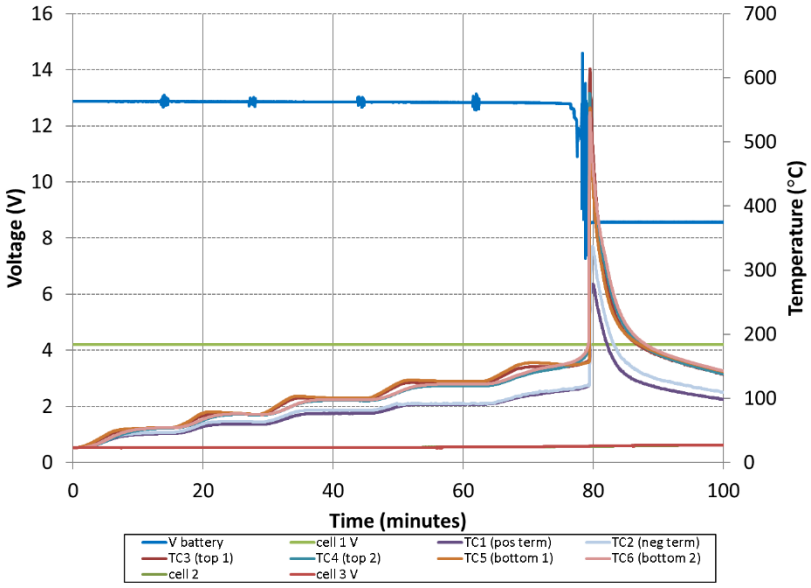

Figure 21 Abuse test run coupled with impedance monitoring and BMS hardware monitoring

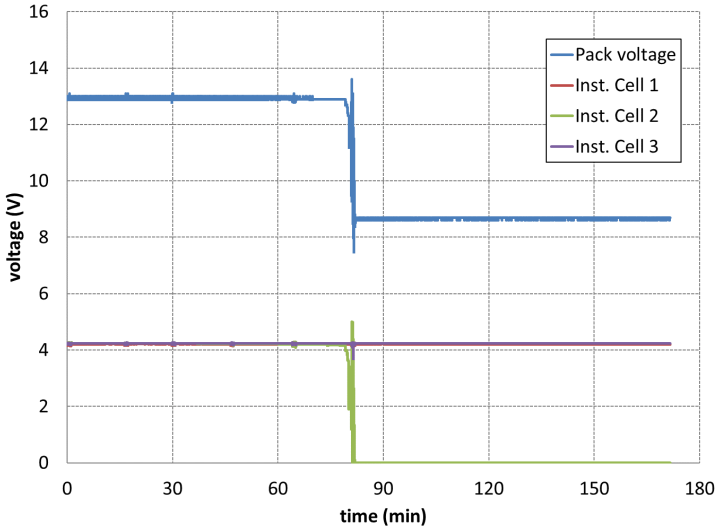

Figure 22 BMS log collected with Figure 21

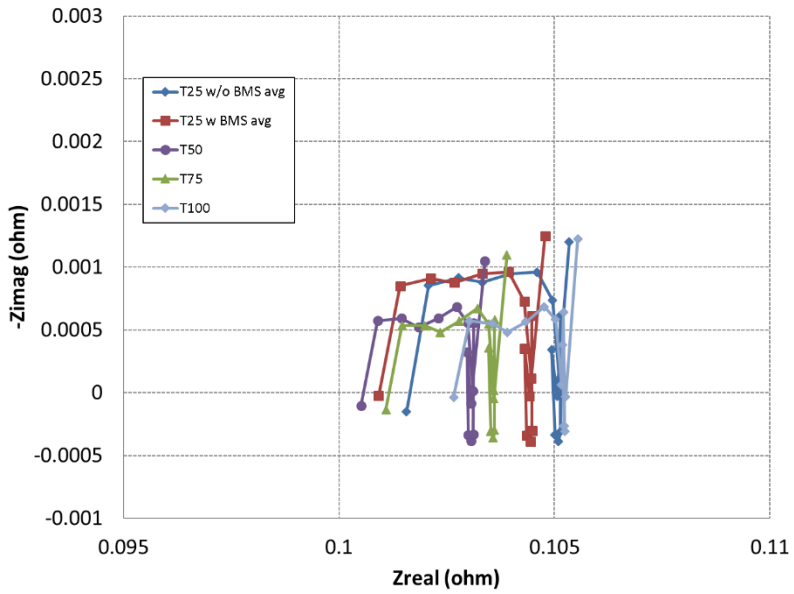

Figure 23 Impedance monitoring up to 100C

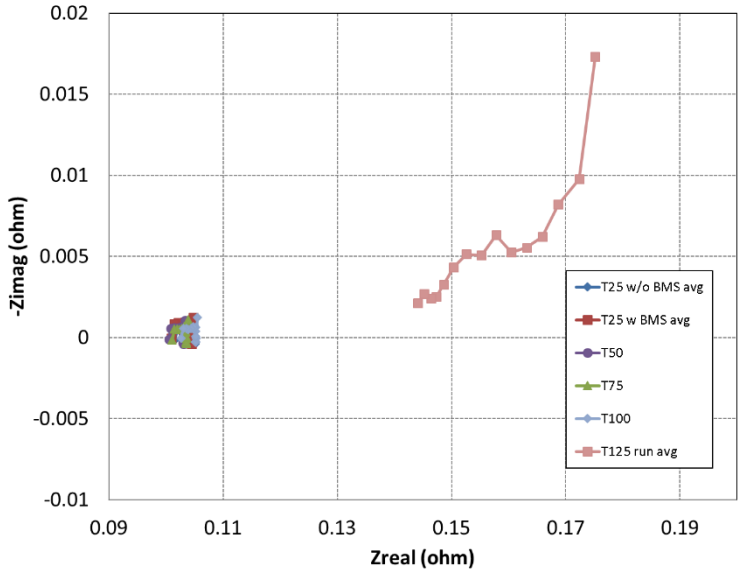

Figure 24 Impedance monitoring up to 125 C

3.2 Evaluating impedance techniques to determine permanent damage of cells

While much of this work has focused on the potential for in-line monitoring, there is also significant potential for post-incident evaluation of a cell or battery. This would allow the electrical probing of cells in an unknown state after they have been potentially exposed to abusive conditions and allow a determination of the relative stability of the cell. This would allow responders to an incident to better determine the appropriate response to the cell or battery in question and guide handling and safety procedures.

Cells were exposed to abusive temperatures (defined as temperatures outside of a cell's normal operating temperature) with impedance monitoring performed before, during and after exposure to said temperature. The cells were allowed to soak at the target temperature to provide enough time to fully equilibrate at the target temperature. Cells that were still operable were cycled as well to establish that any changes observed were likely permanent.

The results for 80 and 100 °C temperature exposures are plotted in Figures 25-27. Figure 25 shows the results after exposing a cell to 100 °C. There is a significant shift in both the internal cell resistance as well as charge transfer resistance after exposure to elevated temperature. There is some increase observed to the charge transfer resistance after the cell is allowed to rest, indicating some transience was present in the immediate aftermath of the test, however after that the impedance measurements remained stable even after 5 charge discharge cycles were applied to the cell. This marks a fairly significant change in the impedance behavior from that observed on the pristine cell.

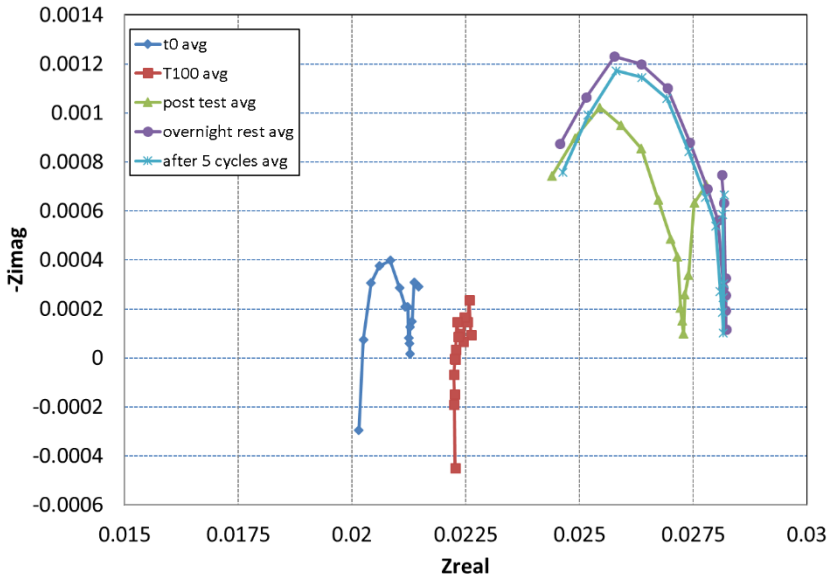

Figure 25 Testing for permanent damage at 100% SOC and 100 °C. This shows the impedance behavior before exposure (t0), at 100 °C (T100), at ambient conditions after exposure (post test), at ambient conditions after an overnight rest (overnight rest) and at ambient conditions after exposure and 5 cycles (after 5 cycles)

Testing before, during and after exposure to an elevated temperature of 80 °C is shown in Figure 26. This data does show some changes after exposure to temperature, with a small change to the internal cell resistance and larger change to the charge transfer resistance. However, this level of change may not be significant enough to be easily identifiable in the field. In particular, the relatively small change in the internal cell resistance may make identification of exposure to this temperature difficult.

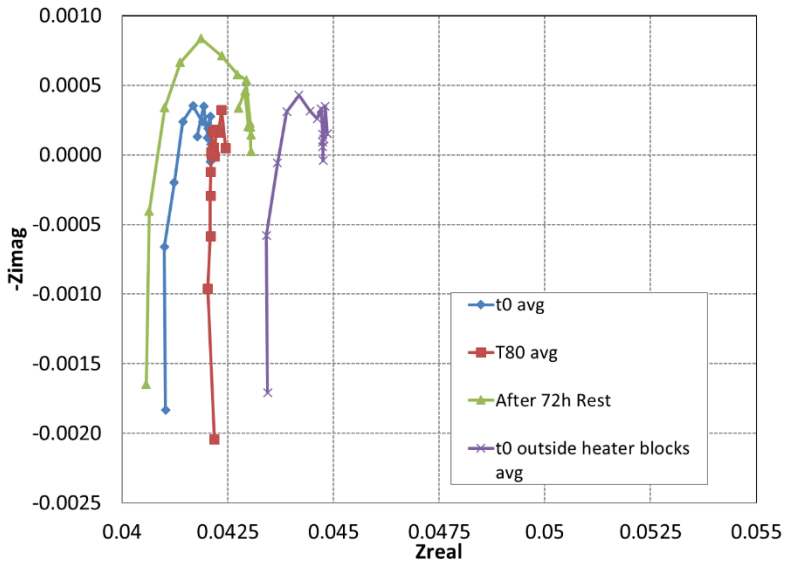

Figure 26 Testing for permanent damage at 100% SOC and 80 °C. This data shows the results before exposure (t0), at 80 °C, and at ambient conditions 72 hours after exposure (after 72h rest).

Exposure to elevated temperature has the potential for creating long term damage to the cell regardless of the state of charge of the cell at the time of exposure. Figure 27 shows this test performed on a cell exposed to 100 °C while at 50% SOC. This shows similar behavior to that seen previously in Figure 26. There are significant changes observed in both internal cell resistance as well as charge transfer resistance. These changes are maintained after charging to 100% SOC as well.

This data combined with the previous data shows that the most significant changes to the cell become present at and above 100 °C. This also provides an opportunity for diagnostic measurements of cells that are in a questionable state. While these impedance scans would not provide a perfect window into a cells history, they could conceivably be applied and compared to the data collected from fresh cells to determine the relative stability of the cell in question. This could help to solve a particular problem with cells after a potentially abusive incident, in determining the relative stability and health of the battery involved. A potentially unstable battery has much stricter handling requirements than one that can be established is relatively healthy. And while this technique would by no means indicate the long term stability and health of a cell, it could conceivably be used to determine the immediate stability (or lack thereof) of a cell or battery in question.

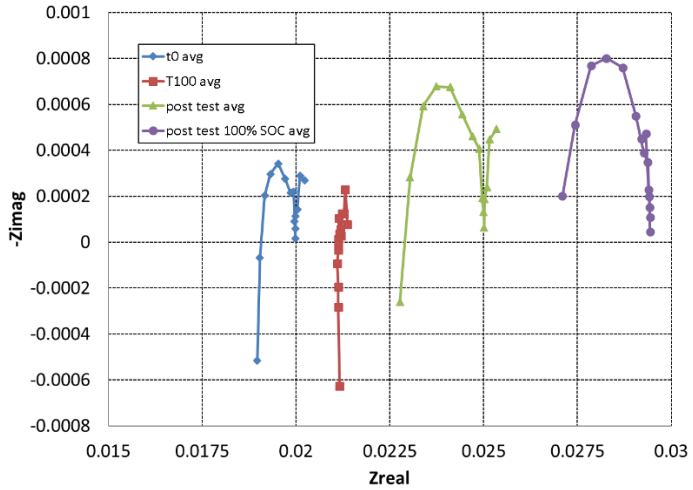

Figure 27 Testing for permanent damage at 50% SOC and 100 °C. This data shows a 50% SOC cell before exposure (t0), at 100 °C, after exposure (post test) and after exposure at 100% SOC (Post test 100% SOC)

3.3 State of stability determination from impedance testing

State of stability (SOS) is a measure of system safety that seeks to predict the likelihood of catastrophic failure. Catastrophic failure can be defined as an uncontrolled thermal runaway of a lithium-ion battery that can involve one or more cells in a battery pack. Quantifying safety is often difficult due to the unpredictability of the time scale of thermal runaway events. Additionally, in large battery packs, it may be difficult to detect potentially unsafe operating conditions until it is too late to mitigate failure. The use of AC impedance measurements can aid in identifying the safety of a battery system by probing the internal electrochemical state of the battery. Because it is an electrical measurement, impedance spectroscopy does not require many sensors for each individual battery; instead, the impedance of the entire battery, or sub-sections of the battery, can be measured and interpreted to assess the SOS of the battery pack.

Mathematically defining SOS requires the identification of health features that accompany catastrophic failure. These features could include the temperature of the battery pack, the voltage of individual cells, or the AC impedance measurements. AC impedance measurements have the potential to provide many different features due to the fact that each impedance sweep contains data points at different frequencies. Each frequency provides unique information about the electrochemical state of the battery, providing many opportunities for detecting anomalous behavior.

3.3.1 Monotonicity of health features

Typically, it is advantageous to have monotonic health features. If a health feature increases and then decreases, it is difficult to determine the SOS because there is not a one-to-one relationship between the operating conditions and the health features. If monotonic health features can be identified, these health features offer an advantage in performing both diagnostics and prognostics.

The interpretation of AC impedance spectra is usually accomplished by fitting an equivalent circuit model, and extracting parameters that describe the charge-transfer resistance, the ohmic resistance, and the diffusive behavior of the battery. These model parameters can then be used as health features. Alternately, it is possible to look at each frequency independently in a purely data-driven approach.

In this approach, we identify health features that (1) are monotonically changing as a function of temperature and (2) have the greatest magnitude of change. While some of the features do not change significantly as a function of temperature or state of charge, others can demonstrate clear monotonic trends. To determine if each of the features is monotonic, the Mann-Kendall statistical test can be performed. The Mann-Kendall test is a non-parametric test that does not make any assumptions about the underlying distribution of the data. The Mann-Kendall test has the following steps:

1.) Perform all possible differences, x_j-x_k, where j>k.
2.) Assign a value of -1, 0, or 1 based on whether the difference is negative, zero, or positive (i.e., sgn(x_j-x_k)).
3.) Calculate $$S = \sum_{j<k} sgn(x_j - x_k)$$
4.) Based on the number of data points, a Z-score can be obtained for the calculated value of S and a statistical hypothesis test can be performed where the null hypothesis is that there is no monotonic trend, and the alternate hypothesis is that there is either a monotonically increasing or decreasing trend.

This procedure is implemented in the sections below to identify monotonic trends in the data; however, instead of performing step 4 to determine statistically whether the trend is monotonic or not, the most monotonic trends can be selected to simplify computation. Additionally, the data is sorted by the largest percentage change to isolate the most meaningful health features.

3.3.2 Thermal Ramp Test

During the thermal ramp test, one of the cells was placed on a thermal block and its temperature was increased at different thermal ramp rates starting at 25°C. The impedance measurement represented the impedance response of the full module, and therefore is the parallel or series combination of each cell's impedance along with any wiring or interconnection impedance. The change in impedance under thermal ramp testing was observed for 1S3P modules (1S3P001 – 1S3P003) as well as 3S1P modules (3S1P004-3S1P005). The Solartron EIS cannot perform real-time scans, and therefore, the scans were taken at regular intervals while the cells were held at rest. The complex magnitude of the impedance was also plotted as a function of temperature.

The impedance spectra for 1S3P001 did not have the same shape or trend as the other packs (1S3P002, 1S3P003). According to discussions with Sandia, long cables led to a lot of noise that overshadowed the true impedance characteristics of the pack. For this reason, 1S3P001 is not being further analyzed.

1S3P002 exhibited a decrease in impedance with increasing temperature. At higher temperatures, the electrolyte resistance will decrease, the kinetic rate of reactions will increase, and thus the charge-transfer resistance will decrease as well. Additionally, at temperatures above 80°C, the solid electrolyte interphase (SEI) layer can breakdown, decreasing the resistance to charge-transfer processes and lithium diffusion. If all 81 of the frequencies are plotted as a function of temperature, the following figure is obtained. The figure contains a lot of information, but it is more helpful to isolate the most consistent and monotonic trends in the data.

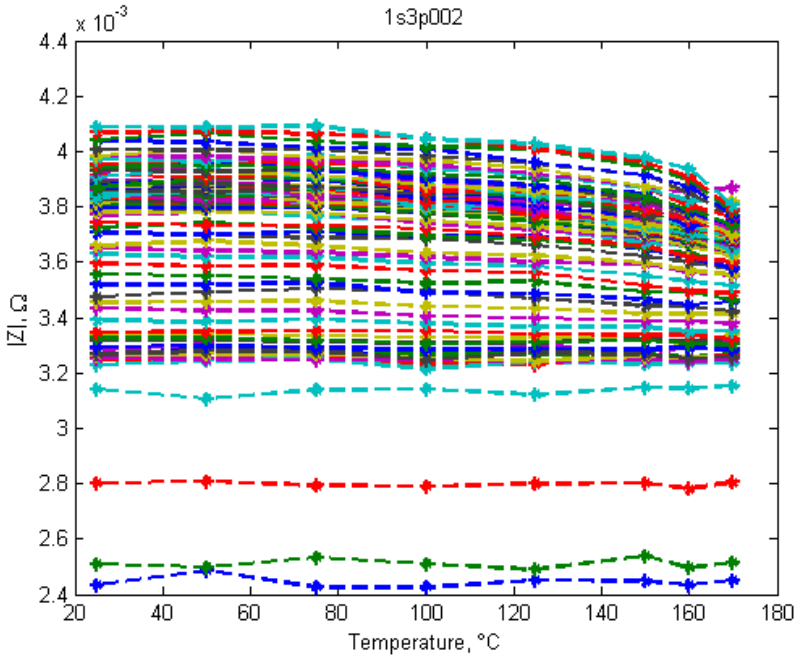

Figure 28 Mann-Kendall testing of various frequencies in a 1S3P string.

The Mann-Kendall test was performed on data from each frequency for the 1S3P002 pack and the top 3 monotonically increasing and top 3 monotonically decreasing trends were plotted. The low frequency values exhibited the largest changes by percentage and have the potential of serving as safety indicators for the battery pack. The mid to high frequencies showed a slight monotonic increasing trend, however, the small percentage increase in the complex magnitude could simply be due to noise.

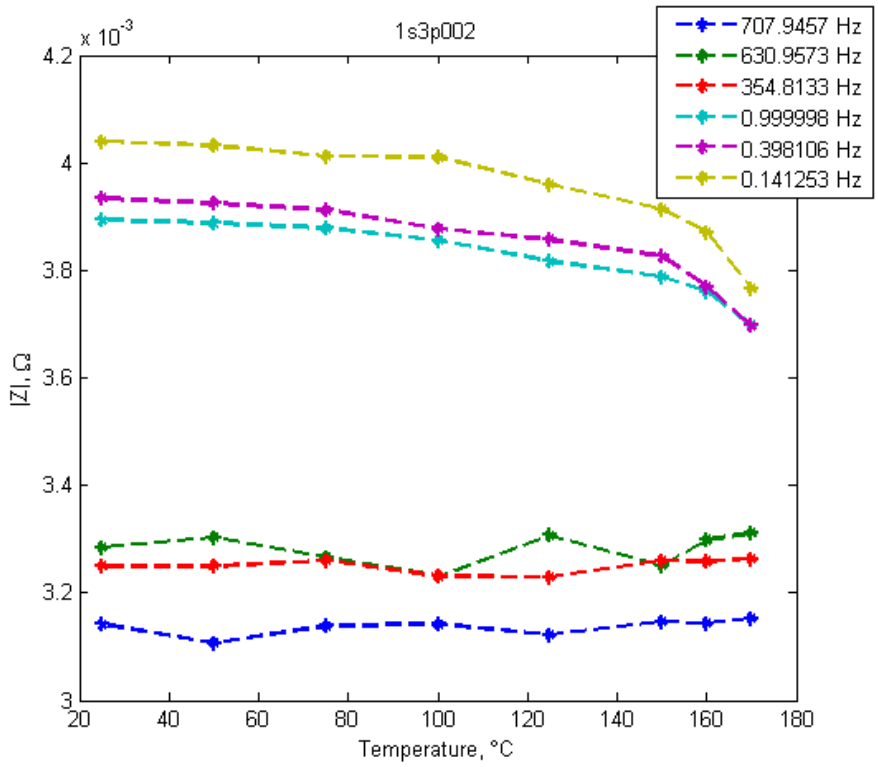

Figure 29 Comparison of low and moderate frequency trends in a 1S3P string.

The Mann-Kendall test was performed on data from 1S3P003, and only monotonically decreasing trends were observed. Therefore, the 6 most monotonically decreasing frequencies are plotted below.

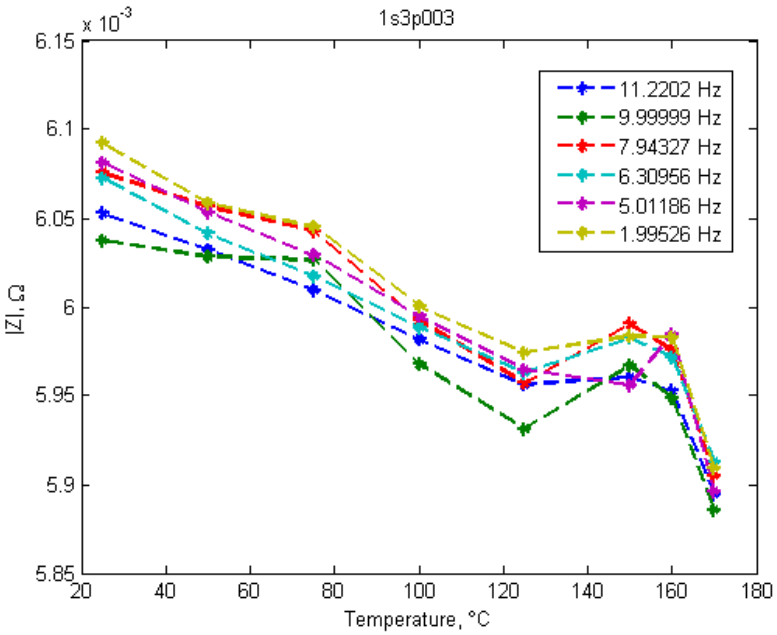

Figure 30 Low frequency behavior in a 1S3P string during thermal ramp testing. A clear transition in behavior can be seen at 120 °C and 160 °C

The data follows a similar trend as the 1S3P002 pack, however, the most monotonically decreasing frequencies occur at higher frequencies. From a practical standpoint, low frequency measurements take longer because a few periods of the AC signal are required. Therefore, it may make more sense to look at mid- to high- frequencies for both 1S3P002 and 1S3P003 even if they are not completely monotonic. For example, the frequency trends for both 1S3P002 and 1S3P003 at 11.22 Hz, 10 Hz, and 7.94 Hz are plotted below. Overall the trends are very similar even though the data from pack 1S3P002 are not completely monotonic. Additional testing could provide confidence bounds on a regression model that captures the relationship between percentage change in the complex magnitude and temperature.

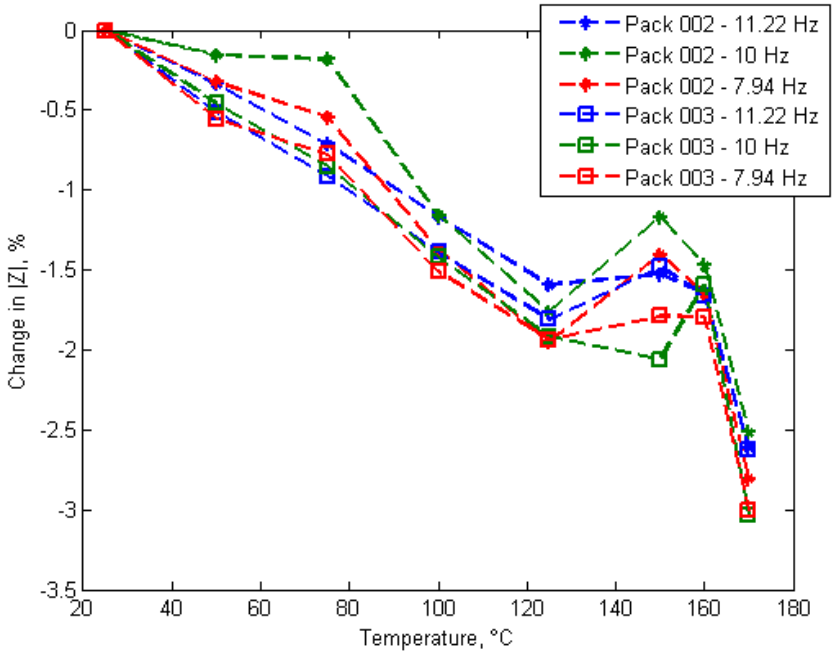

Figure 31 Comparison of multiple packs at similar frequencies. Good agreement is seen amongst multiple 1S3P packs.

Thermal ramp testing was also performed on 3S1P packs (3S1P004 and 3S1P005). In this case, 3 cells are placed in series and one of the cells is subjected to a thermal ramp while impedance measurements are captured at regular intervals. For both packs, monotonically increasing trends were observed. The largest changes occurred above 200°C, however, even if these temperatures are excluded, monotonically increasing changes are observed as seen in the figures below. The increase in impedance is counterintuitive, and this needs to be examined further to explain these results. One possible explanation is that the high frequency data points contain a lot of measurement noise from the experimental setup. However, even the low and mid frequencies have some degree of monotonically increasing trends. Further tests on series connected packs

may be necessary to identify whether monotonically decreasing impedance trends can be identified.

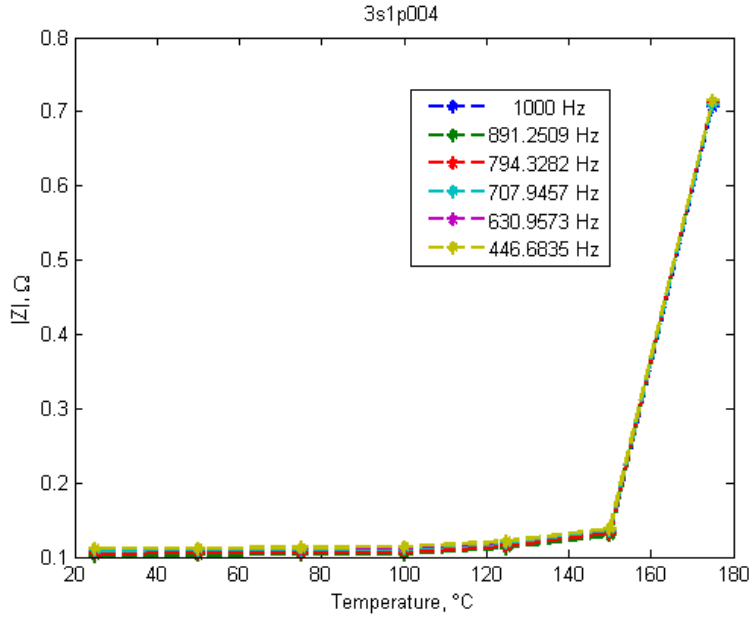

Figure 32 High frequency behavior of a tested 3S1P pack. First changes in behavior are seen above 100 °C, with a significant shift in behvaior above 150 °C.

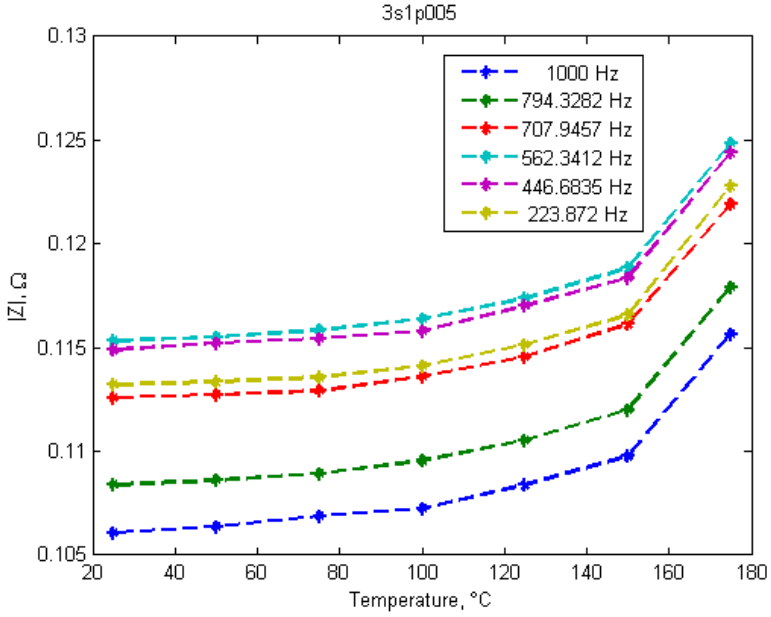

Figure 33 High frequency behavior of a tested 3S1P pack. Similar behavior is seen to that in Figure 32.

3.3.3 Overcharge test

The overcharge tests were performed on three different 3S1P packs (3S1P001 – 3S1P003). Only the first pack, 3S1P001, was charged to 200% state of charge (SOC), whereas the other packs were charged to 180% SOC. All packs followed the same basic trend where the impedance decreases as a function of SOC. For pack 3S1P001, the impedance increases again at 200% SOC, however, this was not confirmed as a consistent trend for other pack samples. The frequencies that displayed the most monotonically decreasing behavior tended to be either low or mid frequency measurements. This is consistent with the results from the thermal ramp tests. For practical purposes, mid frequency signals (e.g., 1-20 Hz) may be the best overall health indicators. This has the advantage of fast measurement time, while providing information about the state of safety (SOS) of the pack.

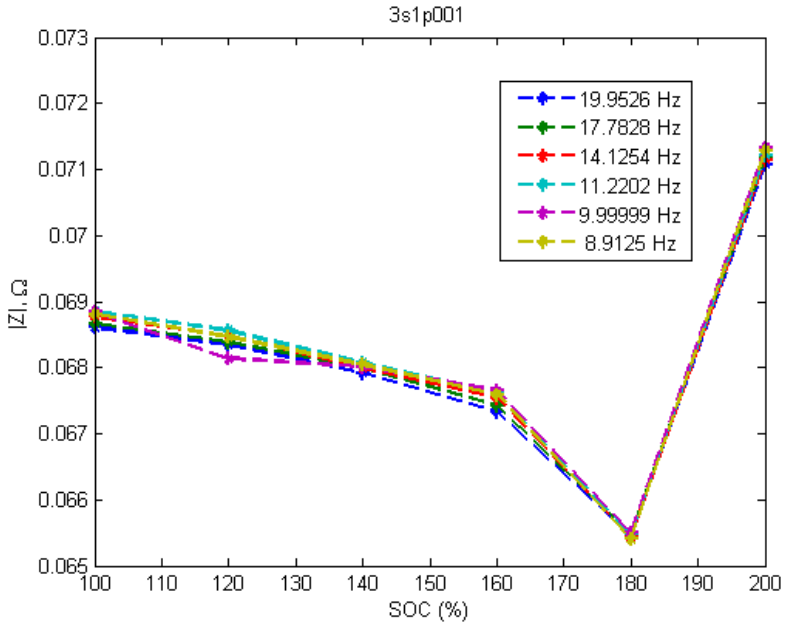

Figure 34 Overcharge applied to a single cell in a 3S1P string. At these moderate frequencies a downward trend is observed up to 160% SOC, with a significant change at 180% SOC.

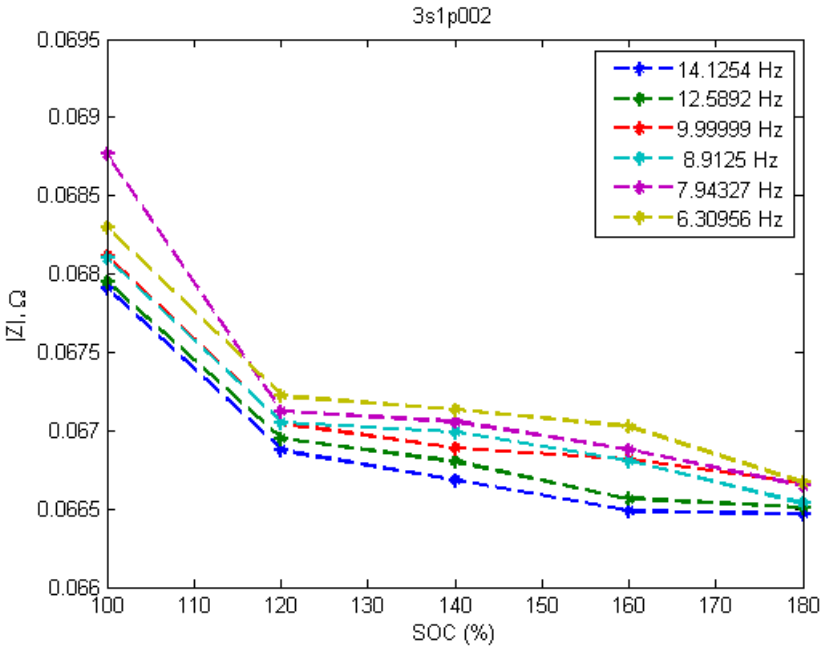

Figure 35 Moderate freuqncy results of a tested 3S1P string. At these frequencies, a change in behavior is noticable at 120% SOC.

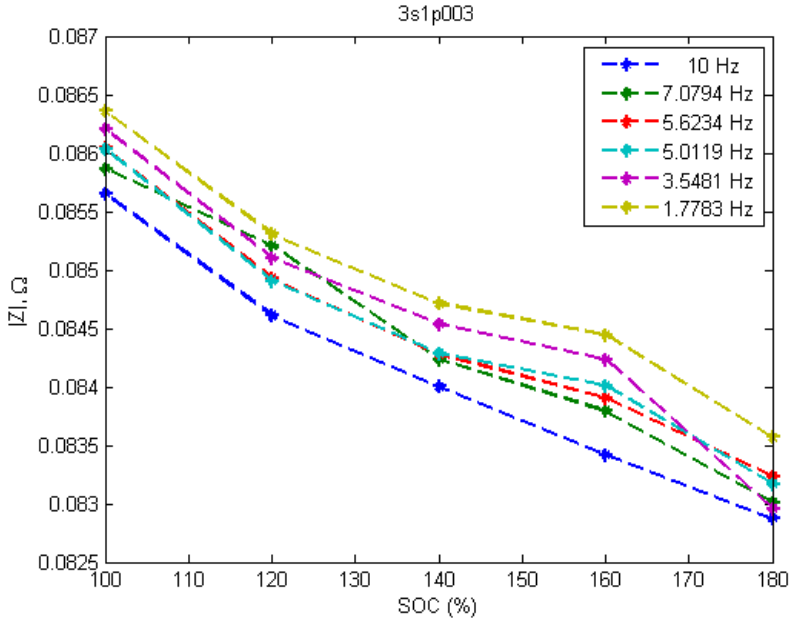

Figure 36 Moderate to low frequency results of a tested 3S1P string. A general decreasing trend in |Z| is observed at these freuqncies.

3.4 SOS Analyais - Continuous AC Impedance Spectroscopy with the Impedance Measurement Box

The Impedance Measurement Box (IMB) was developed through collaboration between Idaho National Laboratory (INL) and Montana Tech. Rather than perform sequential impedance measurements at different frequencies; the IMB performs a single measurement containing multiple frequency signals at once. The real and imaginary impedance values are then calculated from the voltage response. Because the single measurement contains multiple frequencies at once, the measurement time is drastically reduced when compared to traditional sequentially collected AC impedance measurements. As a result of a reduced measurement time, the IMB can be used to collect real-time impedance measurement while a battery is under use. In this part of the study, the IMB was used to measure the impedance of the battery packs during thermal ramp and overcharge testing.

Thermal Ramp Test

During the thermal ramp test, one of the cells was placed on a thermal block and its temperature was increased at different thermal ramp rates starting at 25°C. The impedance was measured once every minute until the cell failed catastrophically. Each measurement was 20 seconds long. The pack labeled 1S3P004 had a single cell whose temperature was increased and scans were taken at regular intervals while the cells were held at rest. The packs labeled 1S3P005, 1S3P006, and 1S3P007 had a single cell that underwent a 5°C/minute thermal ramp, 1S3P009 had a single cell that underwent a 3°C/minute thermal ramp, and 1S3P010 had a single cell that underwent a 2°C/minute thermal ramp.

The impedance measurement box was used to measure the impedance spectra of a 1S3P (1 series, 3 parallel) configuration of cells. The test was repeated for several modules labeled 1S3P004– 1S3P010.

The Mann-Kendall test was performed on pack 1S3P004 and all frequencies exhibited varying degrees of a monotonic decrease in complex magnitude with increasing temperature. The 6 most monotonic trends are plotted below.

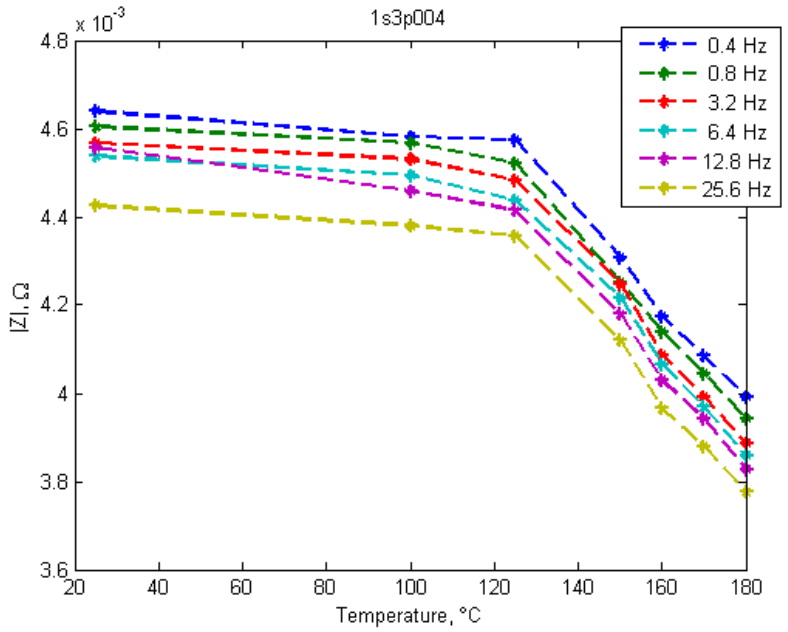

Figure 37 Live thermal ramp testing of a 1S3P string with temperatures allowed to equilibrate. A significant change in cell behavior is observed above 120 °C.

The 6 most monotonic trends are all low to mid-frequencies of the impedance measurement, indicating changes in diffusion and charge-transfer resistance rather than ohmic resistance. The behavior can be separated into two distinct trends. For temperatures below 125°C, the complex impedance magnitude decreases slightly; however, the slope becomes much steeper as the temperature is increased to 180°C. At temperatures above 125°C, the polymer separator has reached its melting point. Although the separator is designed to melt and prevent further ion transport, further increases in temperature can still cause thermal runaway. As the cell was further heated, the separator likely degraded and allowed an internal short circuit between the anode and cathode. Breakdown of the SEI layer at these temperatures and the internal electronic pathways could explain the sudden decrease in charge-transfer resistance and lithium diffusion rates could be increased due to the high temperatures.

For the packs exposed to a 5°C/minute thermal ramp, the state of the battery changed at a fast rate. Because the measurement is taking place over the course of 20 seconds, the temperature is changing by almost 2°C from the beginning of the measurement to the end of the measurement. This will be especially problematic for the low frequency measurements. The plot below shows the 6 most monotonic trends for pack 1S3P005. All trends were monotonically increasing and exhibited a nearly flat slope until a transition around 100°C. This transition occurs close to the melting point of the separator; however, this trend is contrary to what was seen in the 1S3P004 pack. This could be due to the fact that the cell did not have time to stabilize when the impedance measurement was taken, and the increased temperature did not affect the impedance as much as it had for the case where the cell was allowed to rest at each of the temperature points. The same trend was seen for 1S3P007, which also was subjected to a 5°C/minute thermal ramp, but the impedance increased even more dramatically around 160°C.

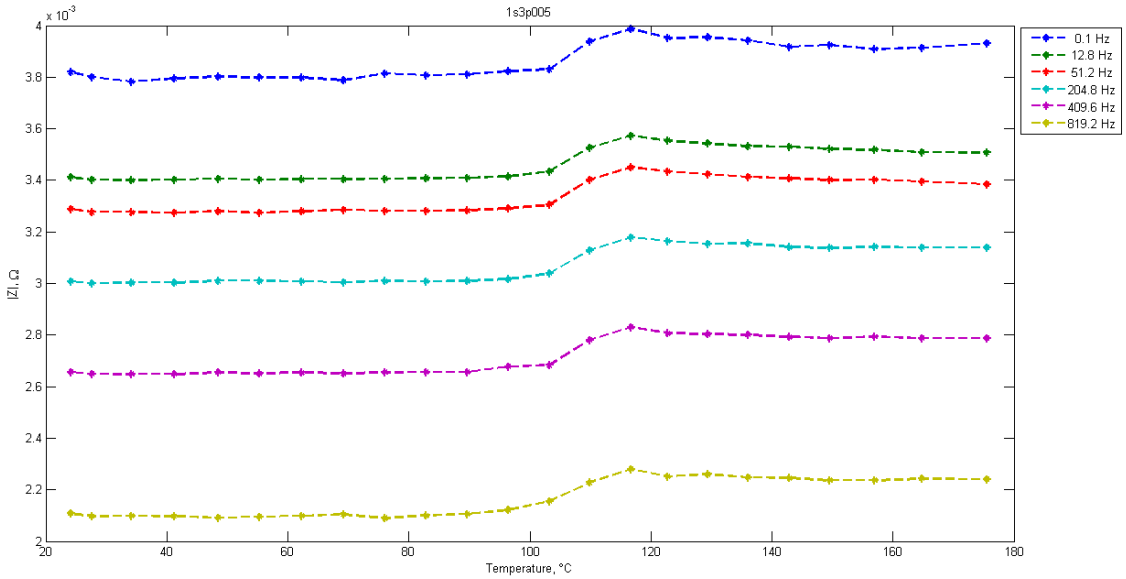

Figure 38 Live testing at a 5 °C/min ramp rate. At this rate temperature transients are too significant to determine a trend when using a 0.1 Hz monitoring frequency.

For pack 1S3P010, the ramp rate was only 2°C/minute, which should result in a more stable IMB measurement due to the small temperature change over the 20 second long measurement. When the Mann-Kendall test was performed, the mid-frequencies exhibited monotonically decreasing trends; however, some of the high and low frequencies exhibited monotonically increasing trends. Looking only at the monotonically decreasing trends, the behavior looks very similar to the results from pack 1S3P004.

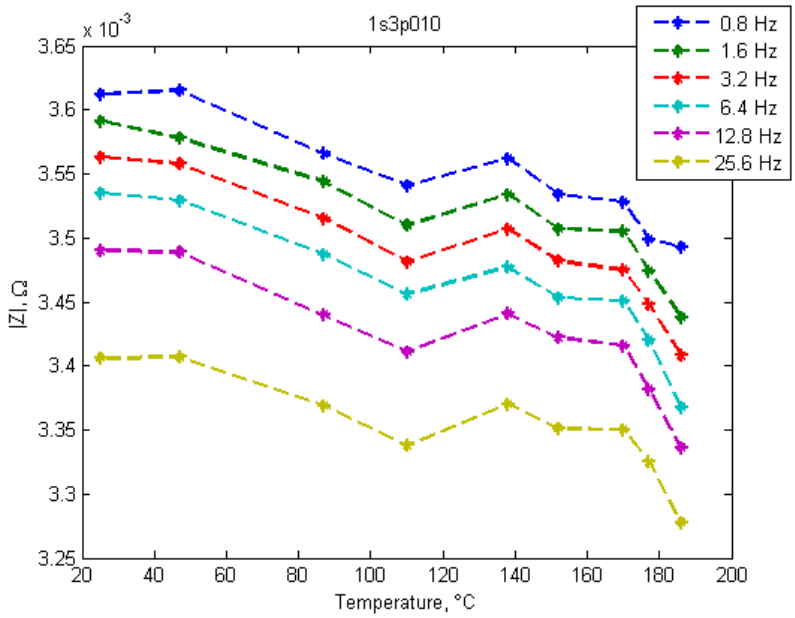

Figure 39 Live monitoring with an applied 2 °C/min ramp rate. This produces results similar to that seen in Figure 31

4. CONCLUSIONS

This phase of this work has focused on 1) the analysis of larger cell formats and configurations that are more representative of electric vehicles, 2) integration of test articles into systems and configurations that are more representative of electric vehicle systems and 3) more detailed analysis of this and previously collected data working towards a useful state of stability measurement. This work was performed with the goal of giving the building blocks necessary to develop the methods explored into a working diagnostic tool kit.

The testing performed so far has shown that it is feasible to have a detectable variable signal in both series and parallel configurations. The variability that has been observed is much more pronounced in series configurations. This is somewhat expected as the natural charge balancing that occurs within parallel strings of cells would likely suppress the response to the impedance measurement. This presents a potential limitation to this method when dealing with a large number of cells in parallel. This may not be ultimately relevant, as current trends are towards small numbers of higher capacity cells, however it is a potential technical challenge that cannot be ignored.

Further analysis has been performed as well to track quantifiable values that can be used as a state of stability determination. This has been used both on aged cells as well as abused cells within small strings. Definite trends have been observed in the scalar impedance value |Z|, which can be used to track cell deterioration and stability loss.

Further, we have demonstrated the potential for identifying a loss of stability in batteries that have been exposed to potentially damaging conditions, but are currently in an unknown state. Further development of these techniques will help to provide an understanding of how cells respond to varying levels of abuse, as well as provide a tool for informing how to best handle cells with an unknown history.

4.1 Technical challenges and future directions

A major challenge that still faces this work is how these techniques will respond as cells and modules approach the size and complexity that are fully relevant for electric vehicle applications. The work currently being performed seeks to answer this question and identify the limits for these techniques, as well as optimize them for larger and more complex systems. The other avenue currently being pursued is to determine if these techniques are significantly impacted by changes to cell chemistry and how the tracked parameters may change.

[Blank page following section.]

5. REFERENCES

1. Abraham, D.P., et al., *Diagnostic examination of thermally abused high-power lithium-ion cells.* Journal of Power Sources, 2006. **161**(1): p. 648-657.
2. Doughty, D.H., et al., *Lithium battery thermal models.* Journal of Power Sources, 2002. **110**(2): p. 357-363.
3. Spotnitz, R.M., et al., *Simulation of abuse tolerance of lithium-ion battery packs.* Journal of Power Sources, 2007. **163**(2): p. 1080-1086.
4. Jeevarajan, J.A., *Limitations of internal protective devices in commercial low capacity cylindrical lithium-ion cells.* Proceedings of the 3rd IAASS Conference 'Building a Safer Space Together', 2009: p. 7 pp.-7 pp.7 pp.
5. Jhu, C.Y., et al., *Self-reactive rating of thermal runaway hazards on 18650 lithium-ion batteries.* Journal of Thermal Analysis and Calorimetry, 2011. **106**(1): p. 159-163.
6. Lamb, J. and C.J. Orendorff, *Evaluation of mechanical abuse techniques in lithium ion batteries.* Journal of Power Sources, 2014. **247**: p. 189-196.
7. Xu, F., et al., *Failure Investigation of LiFePO4 Cells under Overcharge Conditions.* Journal of The Electrochemical Society, 2012. **159**(5): p. A678-A687.
8. Orendorff, C.J., E.P. Roth, and G. Nagasubramanian, *Experimental triggers for internal short circuits in lithium-ion cells.* Journal of Power Sources, 2011. **196**(15): p. 6554-6558.
9. Kozlowski, J.D. *A novel online measurement technique for AC impedance of batteries and other electrochemical systems*. in *Proceedings from the 16th Annual Battery Conference*. 2001.
10. Singh, P., et al., *Fuzzy logic modeling of EIS measurements on lithium-ion batteries.* Electrochimica Acta, 2006. **51**(8-9): p. 1673-1679.
11. Lasia, A., *Comments on the article "An Electrochemical Impedance Measurement Technique Employing Fourier Transform" by J.-S. Yoo and S.-M. Park.* Analytical Chemistry, 2001. **73**(16): p. 4059-4059.
12. Yoo, J.S. and S.M. Park, *An electrochemical impedance measurement technique employing Fourier transform.* Analytical Chemistry, 2000. **72**(9): p. 2035-2041.
13. Yoo, J.S. and S.M. Park, *Reply to comments on the article "An Electrochemical Impedance Measurement Techniques Employing Fourier Transform".* Analytical Chemistry, 2001. **73**(16): p. 4060-4061.
14. Kozlowski, J.D. *Electrochemical cell prognostics using online impedance measurements and model-based data fusion techniques*. in *Proceedings from the IEEE Aerospace Conference*. 2003.
15. Dahn, J.R. and G.M. Ehrlich, *Lithium-Ion Batteries*, in *Linden's Handbook of Batteries*, T.B. Reddy, Editor. 2011, McGraw Hill: New York. p. 26.1-79.
16. Blanke, H., et al., *Impedance measurements on lead-acid batteries for state-of-charge, state-of-health and cranking capability prognosis in electric and hybrid electric vehicles.* Journal of Power Sources, 2005. **144**(2): p. 418-425.
17. Fleischer, C., et al., *On-line adaptive battery impedance parameter and state estimation considering physical principles in reduced order equivalent circuit battery models: Part 1. Requirements, critical review of methods and modeling.* Journal of Power Sources, 2014. **260**(0): p. 276-291.

18. Fleischer, C., et al., *On-line adaptive battery impedance parameter and state estimation considering physical principles in reduced order equivalent circuit battery models part 2. Parameter and state estimation.* Journal of Power Sources, 2014. **262**(0): p. 457-482.
19. Srinivasan, R., et al., *Instantaneous measurement of the internal temperature in lithium-ion rechargeable cells.* Electrochimica Acta, 2011. **56**(17): p. 6198-6204.
20. Schmidt, J.P., et al., *Measurement of the internal cell temperature via impedance: Evaluation and application of a new method.* Journal of Power Sources, 2013. **243**: p. 110-117.
21. Love, C.T. and K. Swider-Lyons, *Impedance Diagnostic for Overcharged Lithium-Ion Batteries.* Electrochemical and Solid-State Letters, 2012. **15**(4): p. A53-A56.
22. Christophersen, J.P., et al., *Crosstalk compensation for a rapid, higher-resolution impedance spectrum measurement.* 2012 IEEE Aerospace Conference, 2012: p. 16 pp.-16 pp.
23. Ramamurthy, A., S. Notani, and S. Bhattacharya, *Advanced lithium ion battery modeling and power stage integration technique.* 2010 IEEE Energy Conversion Congress and Exposition (ECCE), 2010: p. 1485-1492.
24. Christophersen, J.P., et al., *Crosstalk Compensation for a Rapid, Higher-Resolution Impedance Spectrum Measurement.* 2012 Ieee Aerospace Conference, 2012.
25. Morrison, J.L., J.P. Christophersen, and W.H. Morrison, *Universal auto-calibration for a rapid battery impedance spectrum measurement device.* 2014 IEEE Aerospace Conference, 2014: p. 8 pp.-8 pp.

[Blank page following section.]

DISTRIBUTION

[List external recipient names and addresses]

4 Department of Transportation
Attn: Phillip Gorney

4 Idaho National Laboratory
Attn: Jon Christophersen
PO Box 1625
Idaho Falls, ID 83415-3750

[List in order of lower to higher Mail Stop numbers.]

1	MS0613	Joshua Lamb	2546
1	MS0613	Christopher Orendorff	2546
1	MS0613	Thomas Wunsch	2546

[The housekeeping entries are required for all SAND reports.]

1	MS0899	Technical Library	9536 (electronic copy)


Sandia National Laboratories